Since January 2020 Elsevier has created a COVID-19 resource centre with free information in English and Mandarin on the novel coronavirus COVID-19. The COVID-19 resource centre is hosted on Elsevier Connect, the company's public news and information website.

Molecular Cell

Resource

The SARS-CoV-2 RNA interactome

Graphical abstract

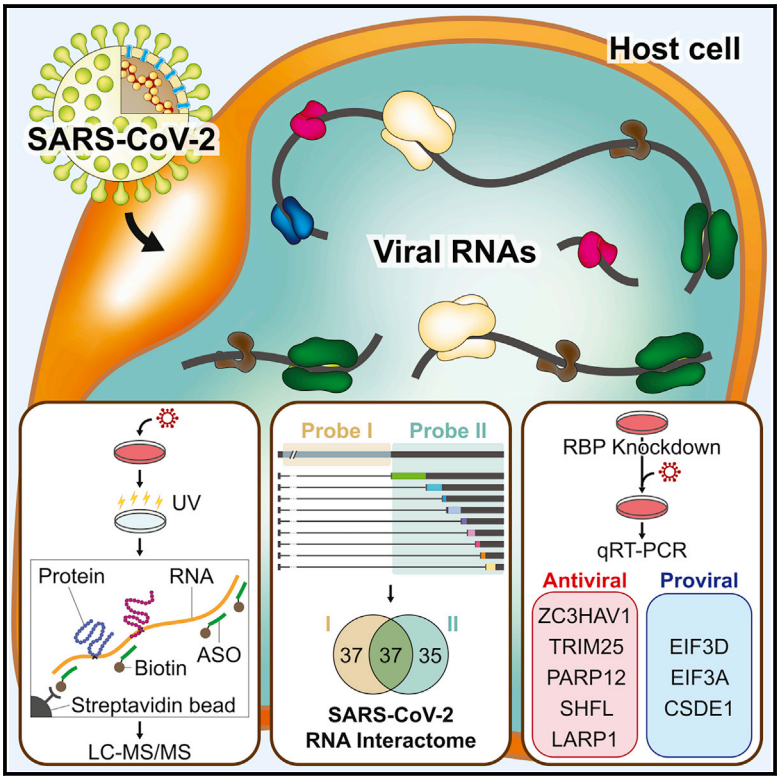

Highlights

- We identify viral and host proteins that directly interact with coronavirus RNAs
- Comparison of SARS-CoV-2 and HCoV-OC43 shows conservation of coronavirus RNA interactome
- This reveals 17 antiviral factors such as LARP1, ZC3HAV1, TRIM25, PARP12, and SHFL
- We also uncover 9 proviral factors hijacked by SARS-CoV-2, including EIF3D and CSDE1

Authors

Sungyul Lee, Young-suk Lee, Yeon Choi, ..., Jeesoo Kim, Jong-Seo Kim, V. Narry Kim

Correspondence

narrykim@snu.ac.kr

In brief

By capturing the ribonucleoprotein (RNP) complex of two coronaviruses SARS-CoV-2 and HCoV-OC43, Lee et al. provide an unbiased and comprehensive list of RNA-binding proteins that physically interact with the viral genome and transcriptome. Loss-of-function experiments stratified the host factors into either proviral or antiviral groups, offering a RNA-centric perspective for understanding the life cycle of coronavirus.

Lee et al., 2021, Molecular Cell *81*, 2838–2850
July 1, 2021
https://doi.org/10.1016/j.molcel.2021.04.022

CellPress

CellPress

Molecular Cell

Resource

The SARS-CoV-2 RNA interactome

Sungyul Lee,[1,2,5] Young-suk Lee,[1,2,3,5] Yeon Choi,[1,2] Ahyeon Son,[1,2] Youngran Park,[1,2] Kyung-Min Lee,[4] Jeesoo Kim,[1,2] Jong-Seo Kim,[1,2] and V. Narry Kim[1,2,6,*]

[1]Center for RNA Research, Institute for Basic Science, Seoul, Republic of Korea
[2]School of Biological Sciences, Seoul National University, Seoul, Republic of Korea
[3]Department of Bio and Brain Engineering, Korea Advanced Institute of Science and Technology (KAIST), Daejeon, Republic of Korea
[4]International Vaccine Institute, Seoul, Republic of Korea
[5]These authors contributed equally
[6]Lead contact
*Correspondence: narrykim@snu.ac.kr
https://doi.org/10.1016/j.molcel.2021.04.022

SUMMARY

SARS-CoV-2 is an RNA virus whose success as a pathogen relies on its abilities to repurpose host RNA-binding proteins (RBPs) and to evade antiviral RBPs. To uncover the SARS-CoV-2 RNA interactome, we here develop a robust ribonucleoprotein (RNP) capture protocol and identify 109 host factors that directly bind to SARS-CoV-2 RNAs. Applying RNP capture on another coronavirus, HCoV-OC43, revealed evolutionarily conserved interactions between coronaviral RNAs and host proteins. Transcriptome analyses and knockdown experiments delineated 17 antiviral RBPs, including ZC3HAV1, TRIM25, PARP12, and SHFL, and 8 proviral RBPs, such as EIF3D and CSDE1, which are responsible for co-opting multiple steps of the mRNA life cycle. This also led to the identification of LARP1, a downstream target of the mTOR signaling pathway, as an antiviral host factor that interacts with the SARS-CoV-2 RNAs. Overall, this study provides a comprehensive list of RBPs regulating coronaviral replication and opens new avenues for therapeutic interventions.

INTRODUCTION

Coronaviruses (CoVs) are a group of enveloped viruses with a nonsegmented, single-stranded, positive-sense (+) RNA genome, which belong to order Nidovirales, family *Coronaviridae*, and subfamily *Coronavirinae* (Lai and Cavanagh, 1997). They are classified into four genera: *Alphacoronavirus* and *Betacoronavirus*, which exclusively infect mammals, and *Gammacoronavirus* and *Deltacoronavirus*, which primarily infect birds (Woo et al., 2012). Human CoVs, such as *Alphacoronavirus* HCoV-229E and *Betacoronavirus* HCoV-OC43, have been known since the 1960s (Hamre and Procknow, 1966) as etiologic agents of the common cold. Recently, the world experienced the emergence of three highly pathogenic human CoV species: severe acute respiratory syndrome CoV (SARS-CoV) in 2002 (Peiris et al., 2003), Middle East respiratory syndrome CoV (MERS-CoV) in 2012 (de Groot et al., 2013), and SARS-CoV-2 in 2019 (Zhou et al., 2020). The most recent one, SARS-CoV-2, causes the respiratory illness known as coronavirus disease 2019 (COVID-19). In March 2020, the outbreak was declared a pandemic by the World Health Organization (WHO).

At the core of the CoV particle, the RNA genome is encapsulated in nucleocapsid (N) protein and surrounded by the viral membrane that contains spike (S) protein, membrane (M) protein, and envelope (E) protein (Lai and Cavanagh, 1997). The coronaviral RNA genome is ~30 kb, which is the longest among RNA viruses, and contains a 5′-cap structure and a 3′ poly(A) tail (Bouvet et al., 2010; Lai and Stohlman, 1981). Upon cell entry, the genomic RNA (gRNA) acts as an mRNA to produce nonstructural proteins (nsps) that are required for viral RNA production (Perlman and Netland, 2009). The ORF1a encodes polypeptide 1a (pp1a; 440–500 kDa), which is cleaved into 11 nsps. The −1 ribosomal frameshift occurs immediately upstream of the ORF1a stop codon, allowing translation of downstream ORF1b, yielding a large polypeptide (pp1ab; 740–810 kDa) that is cleaved into 15 nsps. Together, 16 different nsp fragments are generated to allow subsequent steps of viral RNA synthesis.

After this initial stage of viral translation, the gRNA is used as the template for the synthesis of negative-strand (−) RNA intermediates, which in turn serve as the templates for positive-sense (+) RNA synthesis (Snijder et al., 2016; Sola et al., 2015). Ten different canonical (+) RNA species are produced from the SARS-CoV-2 genome, which include one full-length gRNA and nine subgenomic RNAs (sgRNAs) (Kim et al., 2020a). All canonical viral (+) RNAs share the common 5′ end sequence called the leader sequence and the 3′ end sequences. The sgRNAs are generated via discontinuous transcription, which leads to the fusion between the 5′ leader sequence and the "body" parts containing the downstream open reading frames (Sola et al., 2015) that encode structural proteins (S, E, M, and N) and accessory proteins (3a, 3c, 6, 7a, 7b, 8, and 9b) (Kim et al., 2020a).

To accomplish this, CoVs use unique strategies to evade, modulate, and use the host machinery (Fung and Liu, 2019). For example, the gRNA molecules must be kept in an intricate balance among translation, transcription, and encapsulation by recruiting the right host RNA-binding proteins (RBPs) and

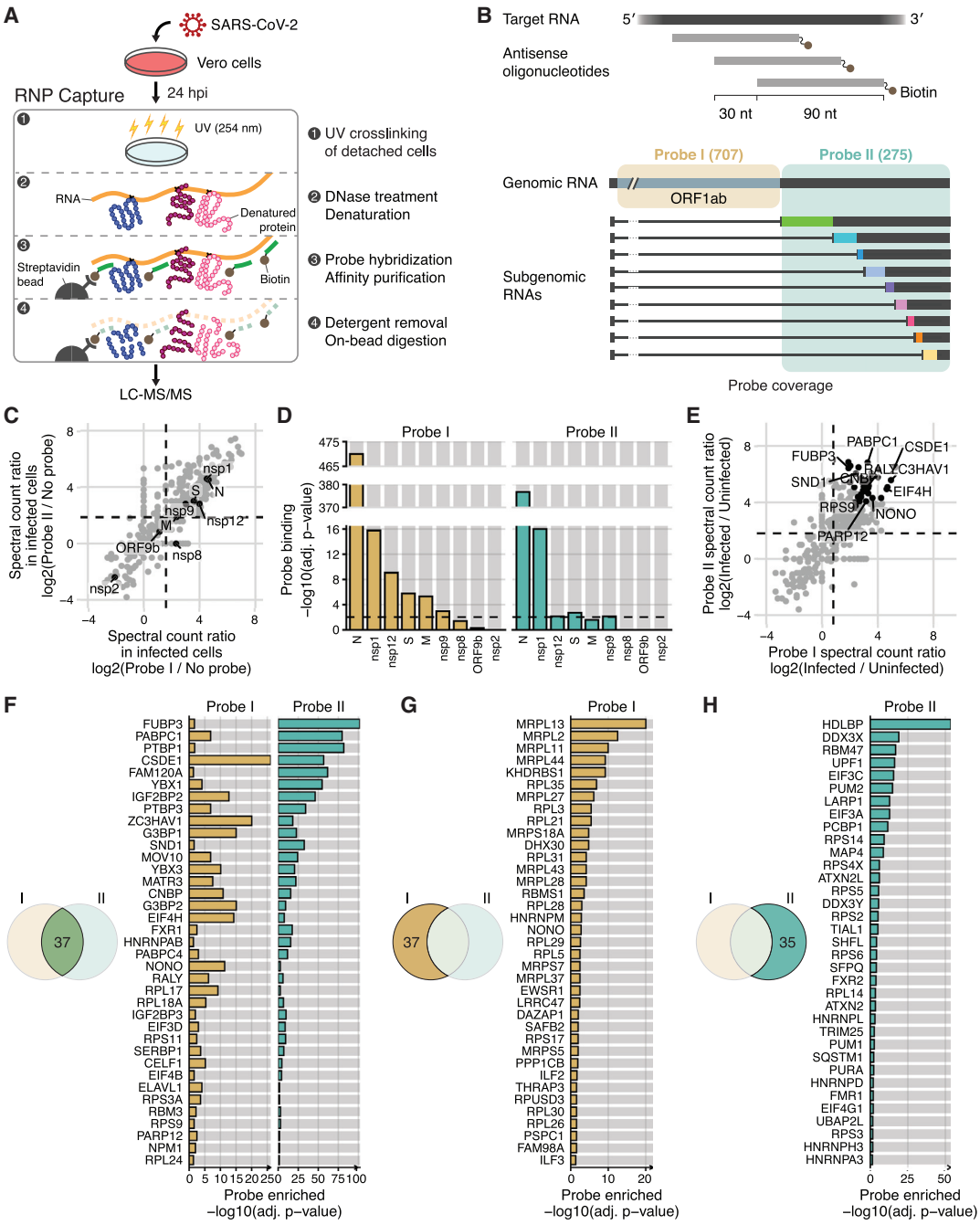

Figure 1. Comprehensive identification host and viral proteins that directly interact with the SARS-CoV-2 RNAs

(A) Schematic of the modified RAP-MS protocol in SARS-CoV-2-infected Vero cells.

(B) Schematic of two separate pools of 90 nt antisense oligonucleotides and their SARS-CoV-2 RNA coverage. The first probe set, "probe I," consists of 707 oligonucleotides that cover the unique region of gRNA, and the second probe set, "probe II," consists of 275 oligonucleotides that cover the common region of gRNA and sgRNAs.

(C) Spectral count ratio of probe I (x axis) and probe II (y axis) experiments over no-probe control in SARS-CoV-2-infected Vero cells (n = 3 technical replicates). Host proteins are marked by gray circles, and viral proteins (n = 9) are marked and labeled in black. The mean spectral count ratio of probe I and of probe II experiments are marked by vertical and horizontal dashed lines, respectively.

(D) Statistical analysis of the quantity of viral proteins over no-probe control (i.e., probe binding). Adjusted (adj.) p values of probe I experiments and of probe II experiments are shown in yellow and green, respectively. Threshold for statistical significance (adj. p value < 0.01) is indicated by horizontal dashed lines.

(E) Spectral count ratio of probe I (x axis) and probe II (y axis) experiments in SARS-CoV-2-infected Vero cells compared with RNP capture experiments in uninfected cells (n = 3 technical replicates). Statistically significant host proteins (n = 37, adj. p value < 0.05) in both probe I and probe II experiments are marked by

(legend continued on next page)

forming specific ribonucleoprotein (RNP) complexes. As host cells counteract by launching RBPs such as RIG-I, MDA5, and Toll-like receptors (TLRs) to recognize and eliminate viral RNAs, the virus needs to evade the immune system using its components to win the arms race between virus and host. How such stealthy devices are genetically coded in this compact RNA genome is yet to be explored (Snijder et al., 2016). Thus, the identification of the RBPs that bind to viral transcripts ("the SARS-CoV-2 RNA interactome") is key to uncovering the molecular rewiring of viral gene regulation and the activation of antiviral defense systems.

Biochemical techniques for studying RNA-protein interactions have been developed (Ramanathan et al., 2019) with advances in protein-centric methods such as CLIP-seq (cross-linking immunoprecipitation followed by sequencing) (Ule et al., 2018). In CLIP-seq experiments, to identify direct RNA-protein interactions, RNP complexes are crosslinked by UV irradiation within cells, after which the protein of interest is immunoprecipitated and the associated RNAs are sequenced (Lee and Ule, 2018; Van Nostrand et al., 2020). More recently, RNA-centric methods have also been developed to profile the mRNA interactome and RNP complexes (Roth and Diederichs, 2015). After UV irradiation, the RNA of interest is purified with oligonucleotide probes, and the crosslinked proteins are identified using mass spectrometry. For example, RNA antisense purification coupled with mass spectrometry (RAP-MS) exhibits compelling evidence of highly confident profiling of proteins that bind to a specific RNA owing to a combination of long hybridization probes and harsh denaturing condition (Engreitz et al., 2013; McHugh et al., 2015).

In this study, we developed a robust RNP capture protocol to define the repertoire of viral and host proteins that associate with the transcripts of CoVs, namely, SARS-CoV-2 and HCoV-OC43. Network and transcriptome analyses combined with knockdown experiments revealed host factors that link the viral RNAs to mRNA regulators and putative antiviral factors.

RESULTS AND DISCUSSION

SARS-CoV-2 RNP purification

To identify the viral and host proteins that directly interact with the genomic and sgRNAs of SARS-CoV-2, we modified the RAP-MS protocol (McHugh and Guttman, 2018), which was developed to profile the interacting proteins of a particular RNA species (Figure 1A). Briefly, virus-infected cells were first detached from culture vessels and irradiated with 254 nm UV to induce RNA-protein crosslink while preserving RNA integrity. Crosslinked cells were treated with DNase and lysed with an optimized buffer condition to homogenize and denature the proteins in high concentration. Pools of biotinylated antisense 90 nt probes were used to capture the denatured RNP complexes in a sequence-specific manner. After stringent washing and detergent removal, the RNP complexes were released and digested by serial Benzonase and on-bead trypsin treatment. These modifications to the RAP-MS protocol enabled robust and sensitive identification of proteins directly bound to the RNA target of interest (see STAR Methods for a detailed explanation). Of note, virus-infected cells were trypsin suspended before UV cross-linking to minimize RNA degradation to capture the intact viral RNAs (see STAR Methods for details).

We designed two separate pools of densely overlapping 90 nt antisense probes to achieve an unbiased perspective of the SARS-CoV-2 RNA interactome (Figure 1B; Table S1). The SARS-CoV-2 transcriptome consists of a gRNA encoding 16 nsps and multiple sgRNAs that encode structural and accessory proteins (Sola et al., 2015). The sgRNAs are more abundant than the gRNA (Kim et al., 2020a). The first pool ("probe I") consisting of 707 oligos tiles every 30 nt across the ORF1ab region (266:21553, NC_045512.2) and thus hybridizes specifically with the gRNA molecules (Figure 1B). The second pool of 275 oligos ("probe II") covers the remaining region (21563:29872, NC_045512.2), which is shared by both the gRNA and sgRNAs.

To first check whether our method specifically captures the viral RNP complexes, we compared the resulting purification from Vero cells infected with SARS-CoV-2 (BetaCoV/Korea/KCDC03/2020) at MOI 0.1 for 24 h (Kim et al., 2020b) by either probe I or probe II. As negative controls, we pulled down without probes ("no probe" control) or with the control probes (for either 18S or 28S rRNA). The protein composition of each RNP sample was distinct as shown by silver staining and western blotting (Figure S1A) with prominent SARS-CoV-2 N protein associated with probes I and II, as expected. Enrichment of SARS-CoV-2 RNAs was confirmed using qRT-PCR (Figure S1B), suggesting that our protocol purifies specific RNP complexes. Note that SARS-CoV-2 gRNA was not enriched in the probe II experiment, hinting at the excess amount of sgRNAs over gRNA in our culture condition.

Comprehensive identification of proteins binding to the SARS-CoV-2 transcripts

We conducted label-free quantification (LFQ) using liquid chromatography with tandem mass spectrometry (LC-MS/MS) and identified 429 host proteins and 9 viral proteins in total (Figure 1C). As highly abundant proteins may nonspecifically co-precipitate during the RNP capture experiment, we statistically modeled this protein background as a multinomial distribution and assessed the probability (i.e., p value) of the quantity of the identified protein in the RNP capture (e.g., probe I) experiment over the protein background of the control (e.g., no-probe) experiment (see STAR Methods for details). This unweighted spectral count analysis resulted in 199 and 220 proteins that are overrepresented in the probe I and probe II sample, respectively (false discovery rate [FDR] < 10%; Table S2). Protein

black circles. Of those, representative host proteins are labeled. The mean spectral count ratio of probe I and of probe II experiments are marked by vertical and horizontal dashed lines, respectively.

(F) Statistical analysis of host proteins enriched in both probe I and probe II experiment (i.e., probe enriched). Adjusted (adj.) p values of probe I experiments and of probe II experiments are shown in yellow and green, respectively. The Venn diagrams represent the number of identified proteins common and distinct between probe I and probe II experiments.

(G and H) Statistical analysis of host proteins enriched (G) in only probe I experiment and (H) in only probe II experiment.

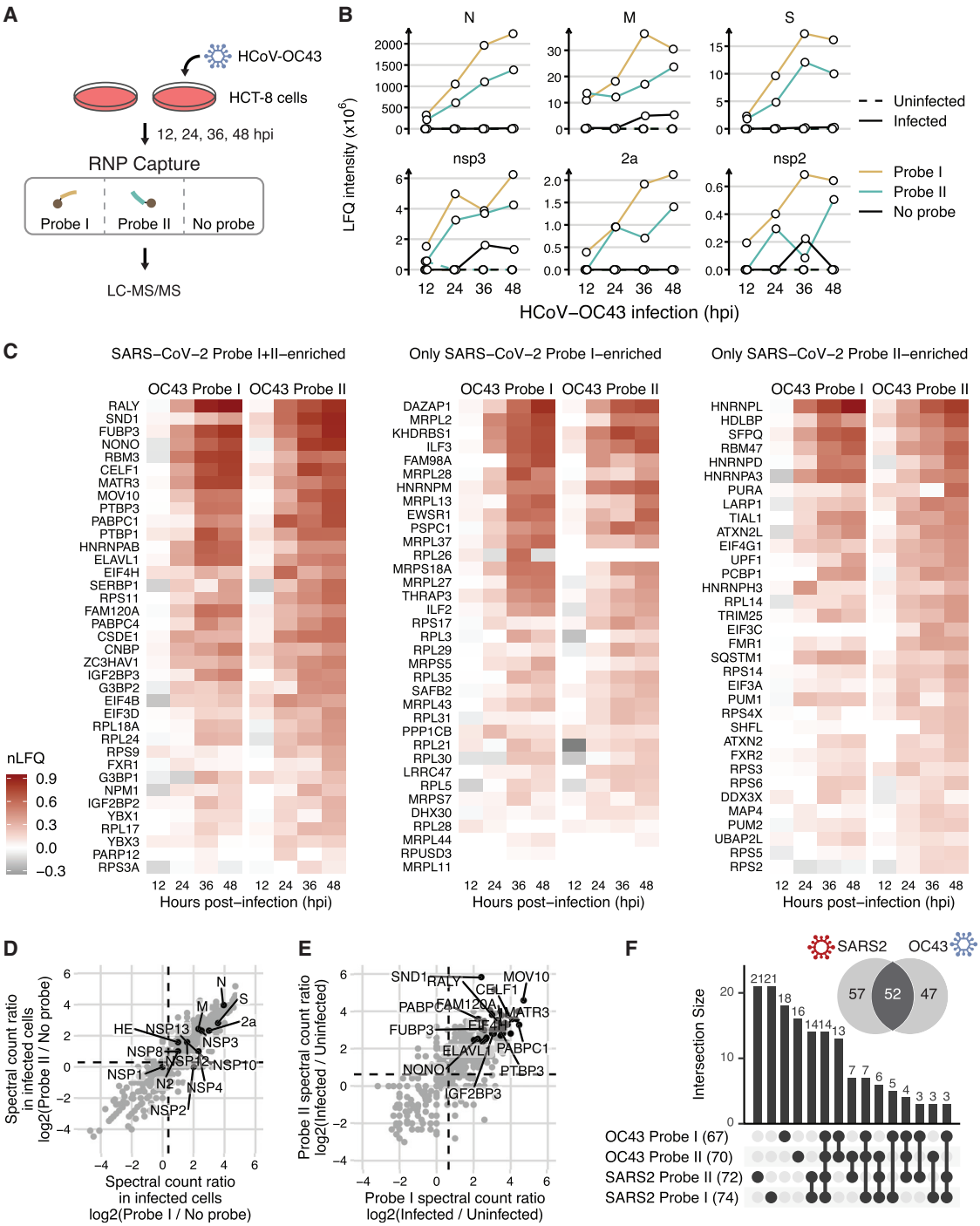

Figure 2. Comparison of SARS-CoV-2 and HCoV-OC43 RNA interactome

(A) Schematic of time course RNP capture experiment in HCoV-OC43-infected HCT-8 cells.

(B) LFQ intensity of abundant viral proteins identified in HCoV-OC43 RNP capture experiment at 12, 24, 36, and 48 h post-infection (hpi).

(C) Heatmap of normalized LFQ intensity (nLFQ) of HCoV-OC43 experiment of host proteins enriched in (left) both SARS-CoV-2 probe I and probe II experiments, (middle) only SARS-CoV-2 probe I experiment, and (right) only SARS-CoV-2 probe II experiment. nLFQ is the $\log_{10}$ fold change over the median LFQ intensity across each probe set (i.e., probe I or probe II). A pseudo-value of 1×10^6 was added to handle missing values.

(D) Spectral count ratio of probe I (x axis) and probe II (y axis) experiments over no-probe control in HCoV-OC43-infected HCT-8 cells of 36 hpi. Host proteins are marked by gray circles, and viral proteins (n = 14) are marked and labeled in black. The mean spectral count ratio of probe I and of probe II experiments are marked by vertical and horizontal dashed lines, respectively.

(legend continued on next page)

domain enrichment analysis revealed that these proteins indeed harbor RNA-binding domains such as RNA recognition motif (RRM) and K homology (KH) domain (Figure S1C). Of note, unlike the cellular mRNA interactome (Castello et al., 2012; Gerstberger et al., 2014), the RNA-binding repertoire of SARS-CoV-2 RNAs showed a depletion of DEAD/DEAH box helicase domains and an enrichment of KH domain.

As for viral proteins, the N protein was the most significantly enriched one, as expected (Figure 1D). The nsp1 protein was also statistically enriched in both probe I and probe II experiments (Figure 1D). Given that probe II precipitates mainly sgRNAs (Figure S1B) because of the abundance of sgRNAs in infected cells (Kim et al., 2020a), nsp1 is likely to interact with both gRNA and sgRNAs. Nsp12, S, M, and nsp9 were detected more with probe I than with probe II, indicating their preferential interaction with gRNAs. CoV nsp9 is a single-strand RNA-binding protein (Egloff et al., 2004; Sutton et al., 2004) essential for viral replication (Miknis et al., 2009). Nsp1 is one of the major virulence factors that suppresses host translation by binding to the 40S ribosomal subunit (Kim et al., 2020a; Thoms et al., 2020). Although nsp1 is studied mostly in the context of translational suppression of host genes (Narayanan et al., 2008), our result hints at the direct role of nsp1 on the transcripts of SARS-CoV-2, corroborating the viral evasion models in which the amino-terminal part of nsp1 interacts with the *cis*-acting RNA hairpin SL1 in the 5′ UTR of SARS-CoV-2, which then dissociates nsp1 from 40S (Banerjee et al., 2020; Shi et al., 2020). Furthermore, our result is not inconsistent with the ribosomal ''gatekeeper'' model in which SL1 induces a structural rearrangement of nsp1 (Tidu et al., 2020). It is also worth mentioning that the nsp2, nsp8, and ORF9b are not enriched in the viral probe experiments, suggesting that these viral proteins do not interact significantly with the viral RNAs.

To delineate the host proteins that are enriched in the SARS-CoV-2 RNP complex, we used an additional negative control experiment with uninfected cells (Figure 1E). In effect, this control provides a conservative background of host proteins as shown by silver staining (Figure S1D). Distributions of peptide length were consistent across technical replicates (Figure S1E), demonstrating the robustness of the ''on-bead'' digestion step. Spectral count analysis against the ''uninfected-probe control'' resulted in 74 and 72 proteins that are enriched in the infected samples with probe I and probe II, respectively (FDR < 5%; Figures 1F–1H). In combination, we define these 109 proteins as the ''SARS-CoV-2 RNA interactome.'' In an independent RNA capture experiment with a control RNA probe targeting 7SL RNAs, the majority of the SARS-CoV-2 interactome (86 of 109 proteins) were preferentially enriched in the viral probe experiments (Figure S1F), demonstrating the specificity of the viral RNA interactome compared with other abundant cytoplasmic RNAs. Thirty-seven host proteins, such as CSDE1 (Unr), EIF4H, FUBP3, G3BP2, PABPC1, and ZC3HAV1, were enriched in both the probe I and probe II RNP capture experiments on infected cells (Figure 1F), thus identifying a robust set of the ''core SARS-CoV-2 RNA interactome.'' Gene Ontology (GO) term enrichment analysis revealed that these host factors are involved in RNA stability control, mRNA function, and viral process (Figure S1G).

Conservation of *Betacoronavirus* RNP complexes

To investigate the evolutionary conservation of the RNA-protein interactions in CoVs, we conducted RNP capture on HCoV-OC43 that belongs to the lineage A of genus *Betacoronavirus* (Figures 2A, S2A, and S2B). HCoV-OC43 shows 54.2% nucleotide homology to SARS-CoV-2 that belongs to lineage B. Two antisense probe sets (i.e., OC43 probe I and OC43 probe II) were designed in a similar manner as in SARS-CoV-2 experiments. OC43 probe I hybridizes only with the gRNA of HCoV-OC43, while probe II can hybridize with both gRNA and sgRNA molecules. As negative controls, the no-probe control on infected cells and the probe control on uninfected cells were used and confirmed by silver staining (Figure S2C). Of note, no substantial differences between time points were found except for increasing protein quantities, which is expected because these are mixed-stage conditions.

Unweighted spectral count analysis against the no-probe control revealed 133, 167, 192, and 160 proteins that are overrepresented in the OC43 probe I experiment at 12, 24, 36, and 48 h post-infection (hpi), respectively (FDR < 10%; Table S3). For the OC43 probe II experiment, 119, 189, 194, and 185 proteins were overrepresented at each respective infection time point (FDR < 10%; Table S4). The analysis of all eight RNP capture experiments resulted in the enrichment of proteins containing canonical RNA-binding domains such as the RRM domain and the KH domain (Figure S2D), indicating the specific precipitation of RBPs.

Fourteen viral proteins, including N, M, and S, were detected within the HCoV-OC43 RNP complexes (Figure 2B; Figure S2E). HCoV-OC43 2a, an accessory protein unique to *Betacoronavirus* lineage A, was also detected, indicating that this protein of unknown function may act as an RBP. The RdRP nsp12 and the papain-like protease nsp3 also appeared, along with the other nsps identified in this experiment. Only a marginal amount of the HCoV-OC43 nsp1 was detected (Figure S2E), implying the functional divergence of nsp1 in *Betacoronavirus* lineages A and B.

Next, we compared the host factors that form the viral RNA interactome of HCoV-OC43 and SARS-CoV-2. All 107 proteins from the SARS-CoV-2 interactome were also detected in the HCoV-OC43 interactome throughout multiple infection time points, except for RBMS1 and DDX3Y (Figure 2C), suggesting a large overlap of RBPs that are common among *Betacoronavirus*. To identify a confident set of the host factors that bind to

(E) Spectral count ratio of probe I (x axis) and probe II (y axis) experiments in HCoV-OC43-infected HCT-8 cells compared with uninfected cells of 36 hpi. Statistically significant host proteins (n = 38, adj. p value < 0.05) in both probe I and probe II experiments are marked by black circles. Of those, representative host proteins are labeled. The mean spectral count ratio of probe I and of probe II experiments are marked by vertical and horizontal dashed lines, respectively.
(F) Upset plot of HCoV-OC43 probe I-enriched (n = 67), HCoV-OC43 probe II-enriched (n = 70), SARS-CoV-2 probe I-enriched (n = 73), and SARS-CoV-2 probe II-enriched (n = 72) proteins. Fourteen host proteins were enriched in all four experiments. The Venn diagrams represent the number of identified proteins common and distinct between the SARS-CoV-2 and OC43 RNA interactome.

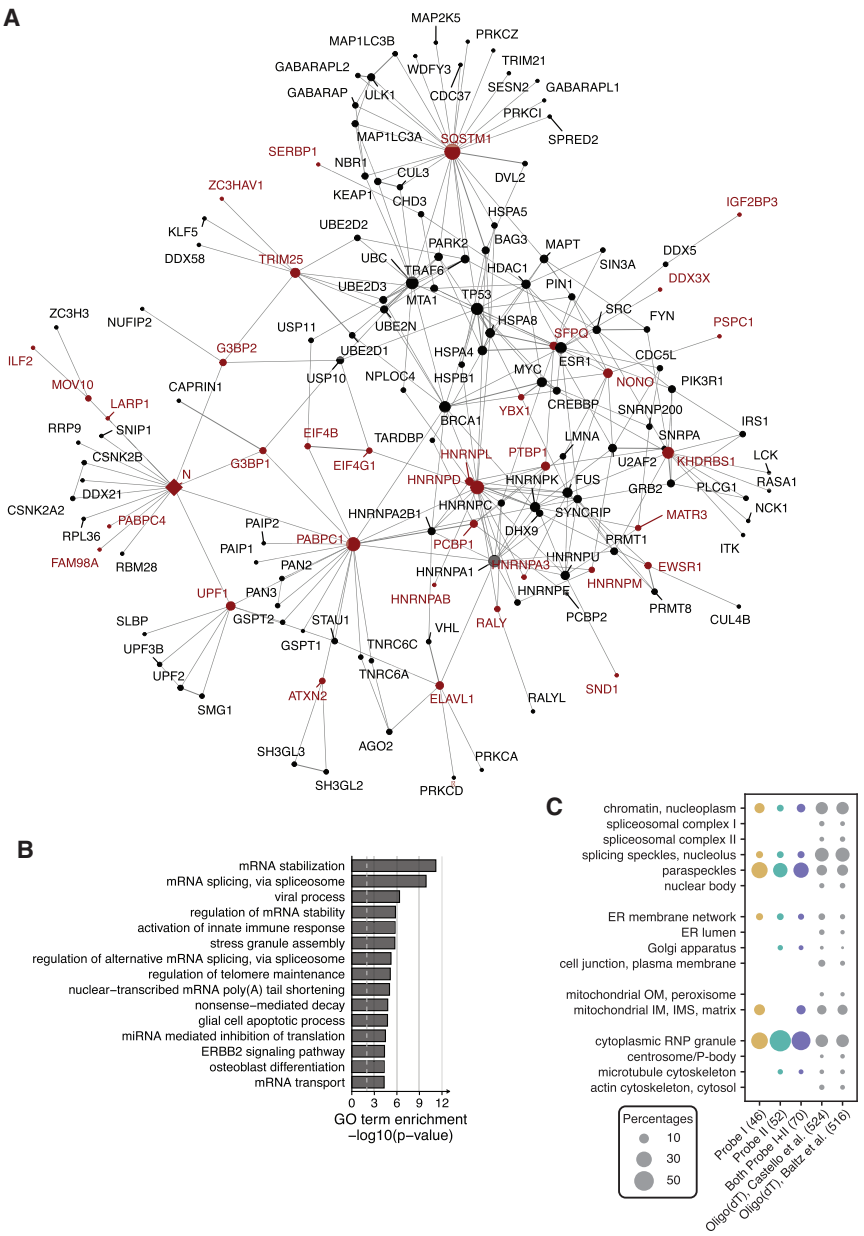

Figure 3. Molecular network of the SARS-CoV-2 RNA interactome

(A) Physical interaction network of SARS-CoV-2 RNA interactome but excluding ribosomal proteins and EIF3 proteins. Host factors are marked in red. Host and viral proteins are marked by circles and diamonds, respectively. The size of the network node is proportional to the number of network edges (i.e., degree) of the node. Largest connected component of the network was chosen for visualization and interpretation.

(B) Gene Ontology biological process term enrichment analysis of proteins retrieved in (A). Threshold for statistical significance (adj. p value < 0.01) is indicated by a vertical dashed line.

(C) Subcellular localization of the SARS-CoV-2 RNA interactome and cellular mRNA interactomes. The number of proteins with localization information is shown in parentheses.

HCoV-OC43 transcripts, we applied our spectral count analysis on the HCoV-OC43 experiment of 36 hpi as a representative (Figure S2A) and conducted statistical analysis in comparison with the no-probe control (Figure 2D; FDR < 10%) and the uninfected-probe control (Figure 2E; FDR < 5%). We identified 67 and 70 host proteins for the HCoV-OC43 probe I and probe II experiments, respectively (Table S5). Thirty-eight proteins were statistically enriched in both probe sets and showed GO term enrichment related to mRNA regulation (Figure S2F). Together, these 99 proteins were defined as "HCoV-OC43 RNA interactome."

Among these 99 proteins, 52 proteins were also identified as the SARS-CoV-2 RNA interactors (Figure 2F) and thus are conserved host components of the *Betacoronavirus* RNA interactome. Among these, 14 proteins (CELF1, EIF4H, ELAVL1, FAM120A, FUBP3, IGF2BP3, MATR3, MOV10, NONO, PABPC1, PABPC4, PTBP3, RALY, SND1, and ZC3HAV1) were detected with both probe sets (I and II) and from both viruses (Figure 2F).

Regulatory landscape of the SARS-CoV-2 RNA interactome

To understand the regulatory significance of the SARS-CoV-2 RNA interactome, we compiled a list of "neighboring" proteins that are known to physically interact with the factors identified in our study (see STAR Methods for details). In particular, we generated a physical interaction network centered (or seeded) by the core SARS-CoV-2 interactome (Figure S3A). Network analysis revealed several network hubs (e.g., NPM1 and PABPC1) and two highly connected network modules: the ribosomal subunits and the EIF3 complex. GO term enrichment analysis resulted in translation-related biological processes (Figure S3B), most likely because of the overrepresentation of ribosomal proteins and subunits of the EIF3 complex, which reflects the active translational status of viral mRNPs.

To achieve a more in-depth functional perspective of the RNA interactome, we reconstructed the physical interaction network with the SARS-CoV-2 RNA interactome but excluding ribosomal proteins and EIF3 proteins (Figure 3A). This analysis identified additional hub proteins such as TRIM25, SQSTM1, and KHDRBS1. GO term enrichment analysis revealed multiple steps of the mRNA life cycle such as mRNA splicing, mRNA export, mRNA stability, and stress granule assembly (Figure 3B), suggesting that these mRNA regulators are co-opted to assist the viral life cycle. Interestingly, we also found GO terms related to

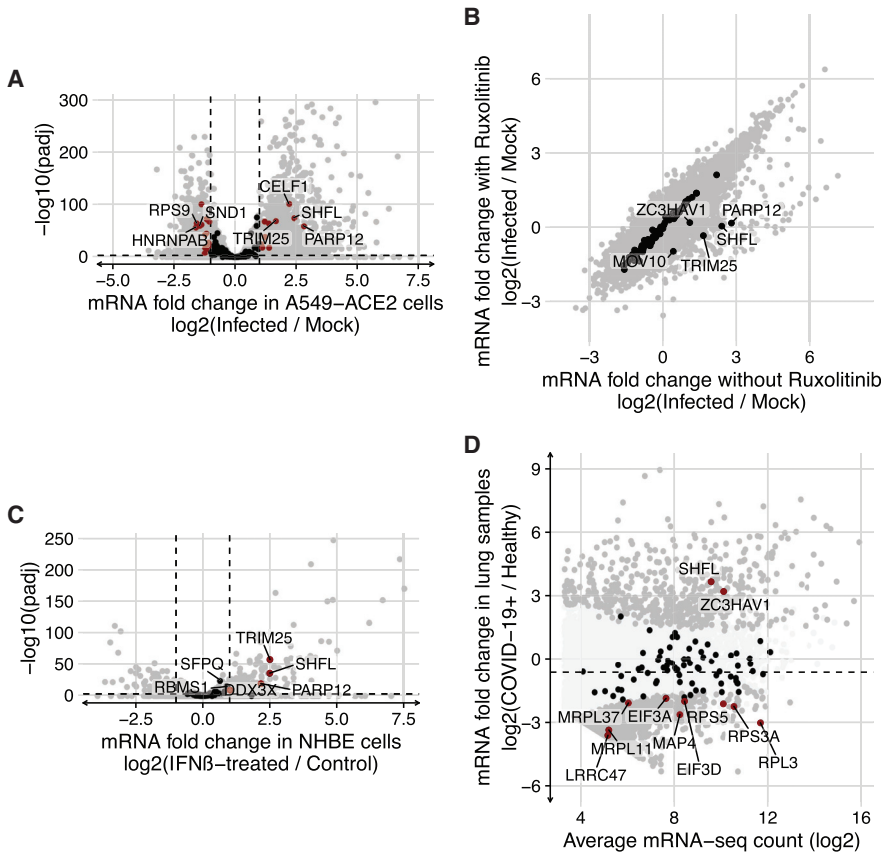

Figure 4. Regulation of the SARS-CoV-2 RNA interactome

(A) Differential expression analysis of ACE2-expressing A549 cells (A549-ACE2) after SARS-CoV-2 infection (MOI = 2.0). mRNA fold changes (FCs) of −1 and 1 are marked by vertical dashed lines. FDR of 1% is marked by a horizontal dashed line. Host genes of the SARS-CoV-2 RNA interactome are marked in red if differentially expressed (FDR < 1% and |FC| > 1) and otherwise in black.

(B) Comparison of mRNA fold change of SARS-CoV-2-infected (MOI = 2.0) A549-ACE2 cells after treatment of ruxolitinib. Host genes of the SARS-CoV-2 RNA interactome are marked in black.

(C) Differential expression analysis of normal human bronchial epithelial (NHBE) cells after IFN-β treatment. Graph notations as in (D).

(D) MA plot of published mRNA-seq data of post-mortem lung samples from COVID-19 patients and healthy lung tissue from uninfected individuals. Mean fold change is marked by a horizontal dashed line. Host genes of the SARS-CoV-2 RNA interactome are marked in red if differentially expressed (FDR < 5%) and otherwise in black. Other differentially expressed genes are in dark gray.

viral processes and innate immune response. In terms of intracellular localization, the SARS-CoV-2 RNA interactome is enriched by proteins localized in the paraspeckle and cytoplasmic RNP granule (e.g., stress granule) compared with the cellular mRNA interactome (Figure 3C) (Baltz et al., 2012; Castello et al., 2012). These observations suggest that the regulatory mechanisms of viral RNAs are distinct from those of host mRNAs, which involve activation of host antiviral machinery and sequestration of viral RNAs.

Another way to gauge the regulatory potential of the SARS-CoV-2 RNA interactome is to examine them in the context of the transcriptional response to viral infection. For example, infected cells recognize the non-cellular RNAs by a number of cytosolic sensors, such as RIG-I (DDX58) and MDA5 (IFIH1), and ultimately induce interferons, which in turn upregulate interferon-stimulated genes (ISGs) through the JAK-STAT pathway (Sa Ribero et al., 2020). Multiple studies have reported the unusually low level of type I/III interferon responses in cell and animal model systems of SARS-CoV-2 infection (Blanco-Melo et al., 2020) and blood biopsy from COVID-19 patients (Hadjadj et al., 2020), indicating active immune evasion by SARS-CoV-2 and supporting the therapeutic potential of timely interferon treatment (Sa Ribero et al., 2020).

To investigate the regulation of the SARS-CoV-2 RNA interactome, we used published transcriptome data of SARS-CoV-2-infected cells (Blanco-Melo et al., 2020). Transcriptome analysis of ACE2-expressing A549 cells revealed host factors of SARS-CoV-2 RNA interactome that are differentially expressed after infection (Figure 4A). Specifically, PARP12, SHFL, CELF1, and TRIM25 are upregulated upon infection. Treatment of ruxolitinib, a JAK1 and 2 inhibitor, in infected cells suppressed the expression of five host factors (MOV10, PARP12, SHFL, TRIM25, and ZC3HAV1) (Figure 4B). TRIM25 and PARP12 are part of the 62 vertebrate core ISGs (Shaw et al., 2017). Interferon-beta (IFN-β) treatment on normal human bronchial epithelial (NHBE) cells induces PARP12, SHFL, and TRIM25 (Figure 4C). Consistently,

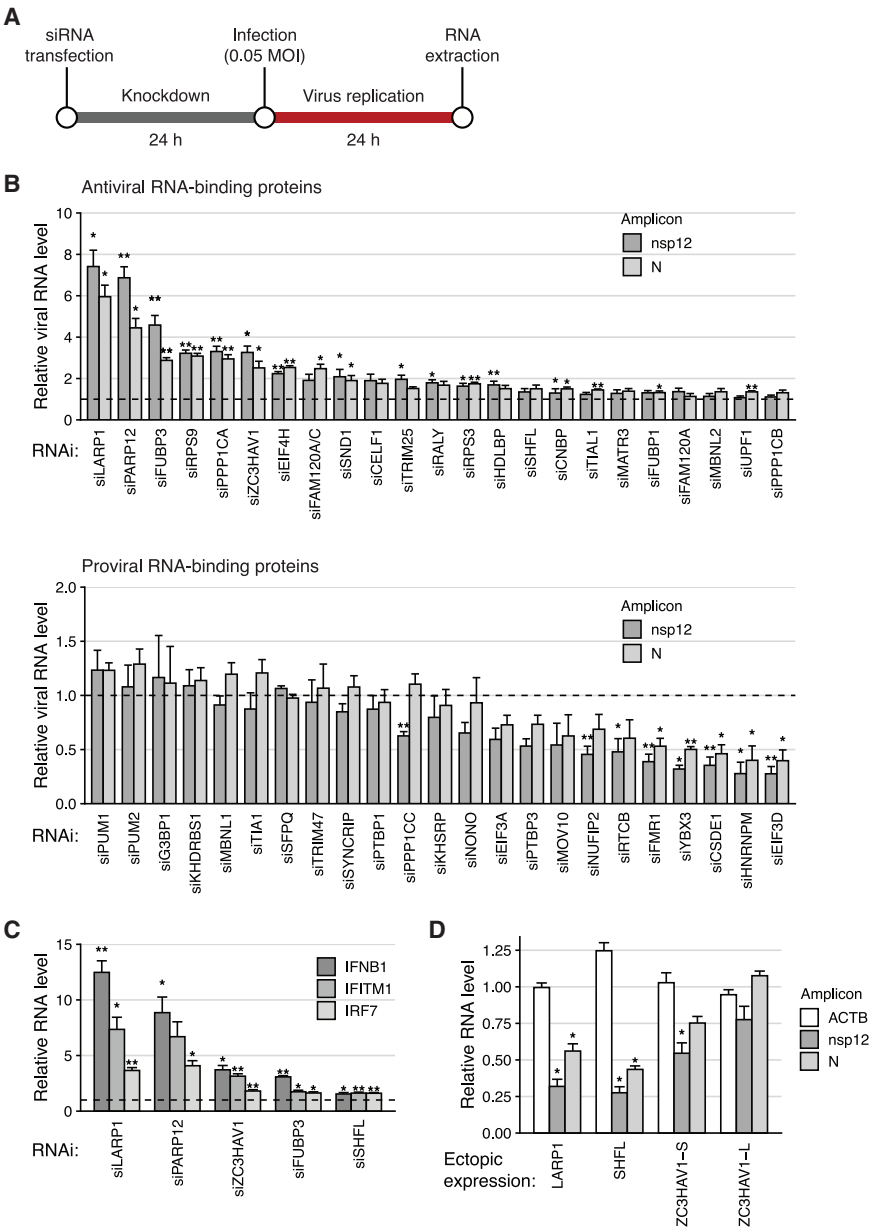

Figure 5. Effects of RBP depletion on viral RNA abundance

(A) Schematic of small interfering RNA (siRNA) knockdown in SARS-CoV-2-infected Calu-3 cells.

(B) Change in gRNA (amplicon nsp12, dark gray) and N sgRNA (amplicon N, light gray) levels after siRNA depletion were measured using qRT-PCR). Data are represented as mean ± SEM (n = 3 or 6 independent experiments). RNA levels in siNC-treated cells were used as negative control and marked by a horizontal dashed line. 18S rRNA was used for normalization. *p < 0.05 and **p < 0.01, two-sided Student's t test.

(C) Relative mRNA levels of β-interferon and ISGs after depletion of antiviral RBPs in SARS-CoV-2-infected Calu-3 cells measured using qRT-PCR. Data are represented as mean ± SEM (n = 3 independent experiments). RNA levels in siNC-treated cells were used as negative control. 18S rRNA was used for normalization. *p < 0.05 and **p < 0.01, two-sided Student's t test.

(D) Relative viral and host RNA levels after ectopic expression of respective FLAG-tagged plasmids (x axis) in SARS-CoV-2-infected HEK293T cells were measured using qRT-PCR. Proteins were expressed 24 h followed by virus infection for another 24 h. Data are represented as mean ± SEM (n = 3 independent experiments). RNA levels are shown relative to that in HEK293T cells transfected with FLAG-tagged GFP plasmids. 28S rRNA was used for total RNA normalization. *p < 0.05, one-sided Student's t test.

proteome analysis of IFN-β-treated cells (Kerr et al., 2020) exhibited an upregulation of PARP12, TRIM25, and ZC3HAV1 (Figure S3C), altogether indicating that JAK-STAT signaling pathway regulates part of the SARS-CoV-2 RNA interactome. Moreover, reanalysis of mRNA sequencing (mRNA-seq) data of post-mortem lung samples from COVID-19 patients (Blanco-Melo et al., 2020) showed upregulation of SHFL and ZC3HAV1 (Figure 4D), highlighting the physiological relevance of SARS-CoV-2 RNP regulation in natural human infection of SARS-CoV-2.

Host factors and functional modules that regulate the SARS-CoV-2 RNAs

To measure the impact of these host proteins on CoV RNAs, we conducted knockdown experiments (Figures S4A and S4B; Table S1) and infected Calu-3 cells with SARS-CoV-2 (Figure 5A; Figure S5A). Calu-3 cells are human lung epithelial cells and often used as a model system for CoV infection (Sims et al., 2008). Strategically, we selected a subset of the SARS-CoV-2 RNA interactome that covers a broad range of functional modules that we identified above: JAK-STAT signaling, mRNA transport, mRNA stability, and translation.

When we depleted RBPs that are induced by SARS-CoV-2 infection or IFN-β treatment, namely, PARP12, TRIM25, ZC3HAV1, CELF1, and SHFL, the viral RNA levels increased (Figure 5B), which suggests that these RBPs may directly suppress CoVs. For instance, ZC3HAV1 (ZAP/PARP13) is an ISG and known to restrict the replication of many RNA viruses such as HIV-1 (*Retroviridae*), Sindbis virus (*Togaviridae*), and Ebola (*Filoviridae*) (Goodier et al., 2015) by promoting RNA degradation (Zhu et al., 2011) and translational repression (Zhu et al., 2012). ZC3HAV1 recognizes CpG and recruits decay factors to degrade HIV RNAs (Takata et al., 2017). TRIM25 is required for activation of ZC3HAV1 (Zheng et al., 2017) by ubiquitin ligation, which depends on RNA-binding activity (Choudhury et al., 2017). Our knockdown results indicate that both ZC3HAV1 and TRIM25 may act as antiviral factors against SARS-CoV-2 (Figure 5B). Consistently, ectopic

expression of the short isoform of ZC3HAV1 (ZC3HAV1-S) showed an antiviral effect against SARS-CoV-2 (Figure 5D). The long isoform (ZC3HAV1-L), which is known to have a stronger effect against some RNA viruses (Kerns et al., 2008), did not have a significant effect on SARS-CoV-2, indicating a difference in specificity among the isoforms (Figure 5D; Figure S5B). Further investigation is needed to understand how ZC3HAV1 and TRIM25 recognize and suppress SARS-CoV-2 transcripts and if SARS-CoV-2 counteracts these antiviral factors.

Other interferon-stimulated RBPs may also be involved in host defense against SARS-CoV-2. SHFL (Shiftless/RyDEN) was induced upon viral infection and interferon treatment and suppressed by JAK inhibitor (Figure 4). SHFL is known to inhibit the translation of diverse RNA viruses, including dengue virus (*Flaviviridae*) and HIV (*Retroviridae*) (Balinsky et al., 2017; Suzuki et al., 2016; Wang et al., 2019). Under our experimental condition, upregulation of viral RNA was modest in SHFL-depleted cells, but further examination is needed, as the knockdown efficiency of ISGs was low in infected cells (Figure S5A). Notably, ectopic expression of SHFL significantly downregulated viral growth (Figure 5D; Figure S5B), demonstrating that SHFL indeed has an antiviral activity against SARS-CoV-2, presumably by blocking ribosomal frameshift in ORF1 translation as reported recently by dual fluorescence frameshift reporters (Schmidt et al., 2021).

Further analyses on other ISGs will also be important for future studies. For instance, PARP12, a cytoplasmic mono-ADP-ribosylation (MARylation) enzyme, is known to have broad antiviral activity against RNA viruses by multiple mechanisms, including blocking cellular RNA translation (Atasheva et al., 2014; Welsby et al., 2014) or triggering proteasome-mediated destabilization of viral proteins (Li et al., 2018). Of note, CoV nsp3 carries a conserved macrodomain that can remove ADP-ribose to reverse the activity of PARP enzymes (Fehr et al., 2015). Knockdown of PARP12 and PARP14 was shown to increase the replication of the macrodomain-deficient mouse hepatitis virus (MHV), which belongs to the lineage A of genus *Betacoronavirus* (Grunewald et al., 2019), which is in line with our knockdown results (Figure 5B). Our RNA interactome data suggest that the RNA-binding activity of PARP12 may help explain the underlying molecular mechanism of its antiviral activity against SARS-CoV-2 transcripts.

We noticed that the coronaviral RNA interactomes are enriched with RBPs with KH domains (Figure S1C; Figure S2D) in comparison with the mRNA interactome. Depletion of FUBP3 (MARTA2) and HDLBP (Vigilin) increased the viral RNA levels (Figure 5B), hinting at a potential antiviral role of certain KH proteins. HDLBP is a conserved protein that contains 14 KH domains and has been implicated in viral translation of dengue virus (Ooi et al., 2019). FUBP3 was enriched in all four RNP capture experiments (i.e., SARS-CoV-2 probes I and II and OC43 probes I and II) (Figure 2C). FUBP3 binds to the 3′ UTR of cellular mRNAs regulating mRNA localization (Blichenberg et al., 1999; Mukherjee et al., 2019). Its connection to the life cycle of CoV is unknown to our knowledge.

Apart from the above RBPs, we identified multiple host factors that have not been previously described in the context of viral infection. Most notably, LARP1 depletion resulted in a substantial upregulation of viral RNAs (Figure 5B). Consistently, ectopic expression of LARP1 led to a reduction of viral growth (Figure 5D; Figure S5B), indicating that LARP1 may have an antiviral function. LARP1 is known to recognize the 5′ terminal oligopyrimidine (TOP) motif which is frequently found in mRNAs encoding ribosomal proteins and translation factors (Fonseca et al., 2015; Tcherkezian et al., 2014). LARP1 represses the translation of 5′ TOP mRNAs in response to metabolic stress, and this repression is relieved by mTORC1-catalyzed phosphorylation of LARP1 (Hong et al., 2017; Lahr et al., 2017).

Not much is known regarding LARP1's role in viral infection. A proteomics study reported that LARP1 interacts with the SARS-CoV-2 N protein (Gordon et al., 2020), although the significance of this interaction remains unknown. SARS-CoV-2 transcripts do not carry the 5′ TOP motif, suggesting that the mechanism of the antiviral activity of LARP1 may be different from that of 5′ TOP mRNA regulation. During the review process of this work, an independent group also confirmed the antiviral function of LARP1 and performed CLIP-seq on LARP1, which revealed that LARP1 may interact with multiple internal pyrimidine-rich sites throughout the body of viral transcripts (Schmidt et al., 2021), complementing the identification of LARP1 in our RNP capture analysis (Figure 1H).

As LARP1 is known to be controlled by mTORC1 (Hong et al., 2017; Lahr et al., 2017), we examined the effect of mTOR inhibitors on SARS-CoV-2 replication. Lately, mTOR inhibitors such as everolimus and omipalisib were proposed as therapeutic options to mitigate the cytokine storm or to protect from lung fibrosis in severe COVID-19 patients (Karam et al., 2020; Klann et al., 2020; Terrazzano et al., 2020). A human cell study reported the inhibition of viral replication by sapanisertib, which targets both mTORC1 and mTORC2 (Schmidt et al., 2021). However, in contrast to previous proposals, we found an increase in SARS-CoV-2 replication after treatment with rapamycin (Figure S5C), which is the prototypic inhibitor specific to mTORC1 (Jacinto et al., 2004). These seemingly opposing results begs the question on how LARP1 regulates viral transcripts without the 5′ TOP motif in a mTORC1-dependent manner. It also needs to be understood how the single/simultaneous inhibition of mTORC1 and mTORC2 affects viral life cycle at the molecular level. In the meantime, a call for caution and rational thinking is needed in terms of the use of mTOR inhibitors for the treatment of COVID-19 patients (Husain and Byrareddy, 2020).

The SARS-CoV-2 RNA interactome includes specific components of the 40S and 60S ribosomal subunits and translational initiation factors (Figures 1F–1H). Knockdown experiments indicated that ribosomal proteins (RPS9 and RPS3) and translation initiation factor EIF4H may have antiviral activities (Figure 5B). EIF4H along with EIF4B is a cofactor for RNA helicase EIF4A (Rogers et al., 2001) whose depletion results in RNA granule formation (Tauber et al., 2020). EIF4H and EIF4B were both identified as the core SARS-CoV-2 RNA interactome (Figure 1F). EIF4H was also reported to interact with SARS-CoV-2 nsp9 (Gordon et al., 2020). Together, our observations implicate that SARS-CoV-2 infection may be closely intertwined with the regulation of ribosome biogenesis, metabolic rewiring, and global translational control.

Regarding proviral factors that may be hijacked by SARS-CoV-2, the translation factors EIF3A, EIF3D, and CSDE1

exhibited proviral effects (Figure 5B). EIF3A is the RNA-binding component of the mammalian EIF3 complex and is evolutionarily conserved along with EIF3B and EIF3C (Masutani et al., 2007). EIF3D is known to interact with mRNA cap and is required for specialized translation initiation (Lee et al., 2016). CSDE1 (Unr) is required for IRES-dependent translation in human rhinovirus (*Picornaviridae*) and poliovirus (*Picornaviridae*) (Anderson et al., 2007; Boussadia et al., 2003). In all, our finding suggests that SARS-CoV-2 may recruit EIF3D and CSDE1 to respectively regulate cap-dependent and IRES-dependent translation initiation (Lee et al., 2017) of SARS-CoV-2 gRNA and sgRNAs.

Our present study reveals a broad spectrum of known antiviral factors, such as TRIM25, ZC3HAV1, PARP12, HDLBP, and SHFL, and also many RBPs whose antiviral functions are unknown, such as LARP1, FUBP3, FAM120A/C, EIF4H, RPS3, RPS9, SND1, CELF1, RALY, and CNBP. Conversely, knockdown of eight host proteins led to a statistically significant decrease in viral RNAs (Figure 5B), suggesting that these host proteins may be proviral factors that are hijacked by the SARS-CoV-2 RNAs. This proviral list includes factors involved in translation, such as EIF3A, EIF3D, and CSDE1, and also unexpected RBPs, such as NUFIP2, RTCB, FMR1, YBX3, and HNRNPM. Of particular interest, the components of tRNA ligase complex (TRLC), such as RTCB, may be involved in SARS-CoV-2 infection. This observation is consistent with a recent finding of the function of RTCB and another TRLC component FAM98A in SARS-CoV-2 infection (Kamel et al., 2020). In sum, this list of proteins reflects constant host-pathogen interactions and opens new avenues to explore unknown mechanisms of viral life cycle and immune evasion.

Along with proteins regulating RNAs, it would also be interesting to consider the possibility of "riboregulation" (Hentze et al., 2018), in which RNA controls its interacting proteins. Dengue virus, for example, uses its sgRNA, called subgenomic flavivirus RNA (sfRNA), to sequester TRIM25 (Chapman et al., 2014). The sgRNA/gRNA ratio is a critical determinant of epidemic potential of dengue virus (Manokaran et al., 2015). Notably, CoVs, including SARS-CoV-2, produce substantial amounts of noncanonical sgRNAs that may serve as noncoding decoys to interact with host RBPs to modulate host immune responses (Kim et al., 2020a).

There are more than 5,100 human clinical studies listed for the treatment of COVID-19 as of March 2021 (ClinicalTrials.gov). The unmet medical need highlights our substantial lack of knowledge of SARS-CoV-2. Thus, redefining antiviral strategies should be contemplated beyond expeditious drug repurposing efforts. So far, collective large and multidisciplinary datasets from viral transcriptome (Kim et al., 2020a), host transcriptional response (Blanco-Melo et al., 2020), ribosome profiling (Finkel et al., 2020), whole proteomics (Bojkova et al., 2020), protein-protein interactions by co-immunoprecipitation (co-IP) (Gordon et al., 2020) and proximity labeling (St-Germain et al., 2020), phosphoproteomics (Bouhaddou et al., 2020), RNA structure (Lan et al., 2020), genome-wide CRISPR screen (Wei et al., 2021), and off-label drug screening (Riva et al., 2020) have all provided invaluable insights of the underlying biology of this novel human CoV. In line with these efforts, our SARS-CoV-2 RNA interactome data, together with the related works reported recently (Flynn et al., 2021; Kamel et al., 2020; Schmidt et al., 2021), will offer insights into the host-viral interaction that regulate the life cycle of CoVs. Data interpretation in the context of publicly available orthogonal information has enabled the identification of proviral and antiviral protein candidates. We expect that further efforts to generate and integrate system-level data will elucidate the pathogenicity of SARS-CoV-2 and introduce new strategies to combat COVID-19.

Limitations of study

Although this comprehensive resource offers new approaches in combating COVID-19, several limitations of this study warrants further investigation. First, the RNA capture experiment was conducted in Vero cells, which are widely used in SARS-CoV-2 experiments but are interferon-deficient kidney epithelial cells from the African green monkey. Therefore, further investigation in a more physiological condition, such as primary human lung epithelial cells, may reveal additional components of the SARS-CoV-2 RNA interactome. Second, interactions between viral RNAs and RBPs are expected to be dynamically regulated at different stages of the viral life cycle, yet our data represent mixed stages and thus lack temporal resolution. Also, the interactions are expected to be modulated in response to interferon, therapeutic drugs, and other cellular signaling pathways, which will be interesting to investigate in the future. Third, the mechanism of action of each member of the SARS-CoV-2 RNA interactome is largely unknown. For example, it is unclear how LARP1 inhibits viral replication by recognizing the SARS-CoV-2 transcriptome, and there is an unexplored missing link between mTOR signaling and LARP1-binding activity on viral RNAs.

STAR★METHODS

Detailed methods are provided in the online version of this paper and include the following:

- KEY RESOURCES TABLE
- RESOURCE AVAILABILITY
  - Lead contact
  - Material availability
  - Data and code availability
- EXPERIMENTAL MODEL AND SUBJECT DETAILS
  - Cell lines
  - Human samples
  - Animal models
- METHOD DETAILS
  - Preparation of antisense oligonucleotide templates
  - Mass production of biotin-labeled ASO
  - Compilation of proteome databases
  - Cell **culture, transfection and virus** infection
  - RNA purification and RT-qPCR
  - Modified RNA antisense purification coupled with mass spectrometry (RAP-MS)
  - LC-MS/MS analysis
- QUANTIFICATION AND STATISTICAL ANALYSIS
  - Statistical analysis for RNP capture experiment
  - Gene Ontology (GO) enrichment analysis
  - Protein-protein interaction network analysis
  - Protein domain enrichment analysis
  - Subcellular localization analysis

SUPPLEMENTAL INFORMATION

Supplemental information can be found online at https://doi.org/10.1016/j.molcel.2021.04.022.

ACKNOWLEDGMENTS

We thank Sun-Je Woo for support in the BL3 laboratory, Kwangmi Moon for advice on BL2 virus culture, and Soohyun Jang for technical support. We also thank Dr. Kwangseog Ahn for sharing reagents. This work would not have been possible without invaluable discussions with members of Narry Kim's lab, particularly Dongwan Kim, Haedong Kim, and Dr. Hyunjoon Kim. The pathogen resource for this study was provided by the National Culture Collection for Pathogens, Korea National Institute of Health for SARS-CoV-2 (NCCP43326), and the Korea Bank for Pathogenic Viruses, Korea University Medical Center for HCoV-OC43 (KBPV-VR-8). This work was supported by the Institute for Basic Science from the Ministry of Science and ICT of Korea (IBS-R008-D1 to V.N.K.) and a BK21 Research Fellowship from the Ministry of Education of Korea (A.S.).

AUTHOR CONTRIBUTIONS

Conceptualization, S.L., Y.L., and V.N.K.; Methodology and experiments, S.L., A.S., and Y.P.; LC-MS/MS, J.K. and J.-S.K.; Data analysis, Y.L. and Y.C.; Manuscript writing, S.L., Y.L., and V.N.K.; Visualization, Y.L., Y.C., and A.S.; Supervision, V.N.K.

DECLARATION OF INTERESTS

We have filed a patent relevant to this paper.

INCLUSION AND DIVERSITY

One or more of the authors of this paper self-identifies as an underrepresented ethnic minority in science.

Received: September 25, 2020
Revised: February 26, 2021
Accepted: April 20, 2021
Published: April 27, 2021

REFERENCES

Alexa, A., Rahnenführer, J., and Lengauer, T. (2006). Improved scoring of functional groups from gene expression data by decorrelating GO graph structure. Bioinformatics *22*, 1600–1607.

Anderson, E.C., Hunt, S.L., and Jackson, R.J. (2007). Internal initiation of translation from the human rhinovirus-2 internal ribosome entry site requires the binding of Unr to two distinct sites on the 5′ untranslated region. J. Gen. Virol. *88*, 3043–3052.

Atasheva, S., Frolova, E.I., and Frolov, I. (2014). Interferon-stimulated poly(ADP-Ribose) polymerases are potent inhibitors of cellular translation and virus replication. J. Virol. *88*, 2116–2130.

Balinsky, C.A., Schmeisser, H., Wells, A.I., Ganesan, S., Jin, T., Singh, K., and Zoon, K.C. (2017). *IRAV* (*FLJ11286*), an interferon-stimulated gene with antiviral activity against dengue virus, interacts with MOV10. J. Virol. *91*, e01606–e01616.

Baltz, A.G., Munschauer, M., Schwanhäusser, B., Vasile, A., Murakawa, Y., Schueler, M., Youngs, N., Penfold-Brown, D., Drew, K., Milek, M., et al. (2012). The mRNA-bound proteome and its global occupancy profile on protein-coding transcripts. Mol. Cell *46*, 674–690.

Banerjee, A.K., Blanco, M.R., Bruce, E.A., Honson, D.D., Chen, L.M., Chow, A., Bhat, P., Ollikainen, N., Quinodoz, S.A., Loney, C., et al. (2020). SARS-CoV-2 disrupts splicing, translation, and protein trafficking to suppress host defenses. Cell *183*, 1325–1339.e21.

Blanco-Melo, D., Nilsson-Payant, B.E., Liu, W.-C., Uhl, S., Hoagland, D., Møller, R., Jordan, T.X., Oishi, K., Panis, M., Sachs, D., et al. (2020). Imbalanced host response to SARS-CoV-2 drives development of COVID-19. Cell *181*, 1036–1045.e9.

Blichenberg, A., Schwanke, B., Rehbein, M., Garner, C.C., Richter, D., and Kindler, S. (1999). Identification of a cis-acting dendritic targeting element in MAP2 mRNAs. J. Neurosci. *19*, 8818–8829.

Bojkova, D., Klann, K., Koch, B., Widera, M., Krause, D., Ciesek, S., Cinatl, J., and Münch, C. (2020). Proteomics of SARS-CoV-2-infected host cells reveals therapy targets. Nature *583*, 469–472.

Bouhaddou, M., Memon, D., Meyer, B., White, K.M., Rezelj, V.V., Correa Marrero, M., Polacco, B.J., Melnyk, J.E., Ulferts, S., Kaake, R.M., et al. (2020). The global phosphorylation landscape of SARS-CoV-2 infection. Cell *182*, 685–712.e19.

Boussadia, O., Niepmann, M., Créancier, L., Prats, A.-C., Dautry, F., and Jacquemin-Sablon, H. (2003). Unr is required in vivo for efficient initiation of translation from the internal ribosome entry sites of both rhinovirus and poliovirus. J. Virol. *77*, 3353–3359.

Bouvet, M., Debarnot, C., Imbert, I., Selisko, B., Snijder, E.J., Canard, B., and Decroly, E. (2010). In vitro reconstitution of SARS-coronavirus mRNA cap methylation. PLoS Pathog. *6*, e1000863.

Castello, A., Fischer, B., Eichelbaum, K., Horos, R., Beckmann, B.M., Strein, C., Davey, N.E., Humphreys, D.T., Preiss, T., Steinmetz, L.M., et al. (2012). Insights into RNA biology from an atlas of mammalian mRNA-binding proteins. Cell *149*, 1393–1406.

Chapman, E.G., Costantino, D.A., Rabe, J.L., Moon, S.L., Wilusz, J., Nix, J.C., and Kieft, J.S. (2014). The structural basis of pathogenic subgenomic flavivirus RNA (sfRNA) production. Science *344*, 307–310.

Choudhury, N.R., Heikel, G., Trubitsyna, M., Kubik, P., Nowak, J.S., Webb, S., Granneman, S., Spanos, C., Rappsilber, J., Castello, A., and Michlewski, G. (2017). RNA-binding activity of TRIM25 is mediated by its PRY/SPRY domain and is required for ubiquitination. BMC Biol. *15*, 105.

Cox, J., and Mann, M. (2008). MaxQuant enables high peptide identification rates, individualized p.p.b.-range mass accuracies and proteome-wide protein quantification. Nat. Biotechnol. *26*, 1367–1372.

Cox, J., Neuhauser, N., Michalski, A., Scheltema, R.A., Olsen, J.V., and Mann, M. (2011). Andromeda: a peptide search engine integrated into the MaxQuant environment. J. Proteome Res. *10*, 1794–1805.

de Groot, R.J., Baker, S.C., Baric, R.S., Brown, C.S., Drosten, C., Enjuanes, L., Fouchier, R.A.M., Galiano, M., Gorbalenya, A.E., Memish, Z.A., et al. (2013). Middle East respiratory syndrome coronavirus (MERS-CoV): announcement of the Coronavirus Study Group. J. Virol. *87*, 7790–7792.

Egloff, M.-P., Ferron, F., Campanacci, V., Longhi, S., Rancurel, C., Dutartre, H., Snijder, E.J., Gorbalenya, A.E., Cambillau, C., and Canard, B. (2004). The severe acute respiratory syndrome-coronavirus replicative protein nsp9 is a single-stranded RNA-binding subunit unique in the RNA virus world. Proc. Natl. Acad. Sci. U S A *101*, 3792–3796.

El-Gebali, S., Mistry, J., Bateman, A., Eddy, S.R., Luciani, A., Potter, S.C., Qureshi, M., Richardson, L.J., Salazar, G.A., Smart, A., et al. (2019). The Pfam protein families database in 2019. Nucleic Acids Res. *47* (D1), D427–D432.

Engreitz, J.M., Pandya-Jones, A., McDonel, P., Shishkin, A., Sirokman, K., Surka, C., Kadri, S., Xing, J., Goren, A., Lander, E.S., et al. (2013). The Xist lncRNA exploits three-dimensional genome architecture to spread across the X chromosome. Science *341*, 1237973.

Fehr, A.R., Athmer, J., Channappanavar, R., Phillips, J.M., Meyerholz, D.K., and Perlman, S. (2015). The nsp3 macrodomain promotes virulence in mice with coronavirus-induced encephalitis. J. Virol. *89*, 1523–1536.

Finkel, Y., Mizrahi, O., Nachshon, A., Weingarten-Gabbay, S., Yahalom-Ronen, Y., Tamir, H., Achdout, H., Melamed, S., Weiss, S., Israely, T., et al. (2020). The coding capacity of SARS-CoV-2. bioRxiv. https://doi.org/10.1101/2020.05.07.082909.

Flynn, R.A., Belk, J.A., Qi, Y., Yasumoto, Y., Wei, J., Alfajaro, M.M., Shi, Q., Mumbach, M.R., Limaye, A., DeWeirdt, P.C., et al. (2021). Discovery and

functional interrogation of SARS-CoV-2 RNA-host protein interactions. Cell. Published online March 11, 2021. https://doi.org/10.1016/j.cell.2021.03.012.

Fonseca, B.D., Zakaria, C., Jia, J.-J., Graber, T.E., Svitkin, Y., Tahmasebi, S., Healy, D., Hoang, H.-D., Jensen, J.M., Diao, I.T., et al. (2015). La-related protein 1 (LARP1) represses terminal oligopyrimidine (TOP) mRNA translation downstream of mTOR complex 1 (mTORC1). J. Biol. Chem. *290*, 15996–16020.

Fung, T.S., and Liu, D.X. (2019). Human coronavirus: host-pathogen interaction. Annu. Rev. Microbiol. *73*, 529–557.

Gene Ontology Consortium (2001). Creating the Gene Ontology resource: design and implementation. Genome Res. *11*, 1425–1433.

Gerstberger, S., Hafner, M., and Tuschl, T. (2014). A census of human RNA-binding proteins. Nat. Rev. Genet. *15*, 829–845.

Go, C.D., Knight, J.D.R., Rajasekharan, A., Rathod, B., Hesketh, G.G., Abe, K.T., Youn, J.-Y., Samavarchi-Tehrani, P., Zhang, H., Zhu, L.Y., et al. (2019). A proximity biotinylation map of a human cell. bioRxiv. https://doi.org/10.1101/796391.

Goodier, J.L., Pereira, G.C., Cheung, L.E., Rose, R.J., and Kazazian, H.H., Jr. (2015). The broad-spectrum antiviral protein ZAP restricts human retrotransposition. PLoS Genet. *11*, e1005252.

Gordon, D.E., Jang, G.M., Bouhaddou, M., Xu, J., Obernier, K., White, K.M., O'Meara, M.J., Rezelj, V.V., Guo, J.Z., Swaney, D.L., et al. (2020). A SARS-CoV-2 protein interaction map reveals targets for drug repurposing. Nature *583*, 459–468.

Grunewald, M.E., Chen, Y., Kuny, C., Maejima, T., Lease, R., Ferraris, D., Aikawa, M., Sullivan, C.S., Perlman, S., and Fehr, A.R. (2019). The coronavirus macrodomain is required to prevent PARP-mediated inhibition of virus replication and enhancement of IFN expression. PLoS Pathog. *15*, e1007756.

Hadjadj, J., Yatim, N., Barnabei, L., Corneau, A., Boussier, J., Smith, N., Péré, H., Charbit, B., Bondet, V., Chenevier-Gobeaux, C., et al. (2020). Impaired type I interferon activity and inflammatory responses in severe COVID-19 patients. Science *369*, 718–724.

Hamre, D., and Procknow, J.J. (1966). A new virus isolated from the human respiratory tract. Proc. Soc. Exp. Biol. Med. *121*, 190–193.

Hentze, M.W., Castello, A., Schwarzl, T., and Preiss, T. (2018). A brave new world of RNA-binding proteins. Nat. Rev. Mol. Cell Biol. *19*, 327–341.

Hong, S., Freeberg, M.A., Han, T., Kamath, A., Yao, Y., Fukuda, T., Suzuki, T., Kim, J.K., and Inoki, K. (2017). LARP1 functions as a molecular switch for mTORC1-mediated translation of an essential class of mRNAs. eLife *6*, e25237.

Husain, A., and Byrareddy, S.N. (2020). Rapamycin as a potential repurpose drug candidate for the treatment of COVID-19. Chem. Biol. Interact. *331*, 109282. https://doi.org/10.1016/j.cbi.2020.109282.

Jacinto, E., Loewith, R., Schmidt, A., Lin, S., Rüegg, M.A., Hall, A., and Hall, M.N. (2004). Mammalian TOR complex 2 controls the actin cytoskeleton and is rapamycin insensitive. Nat. Cell Biol. *6*, 1122–1128.

Kamel, W., Noerenberg, M., Cerikan, B., Chen, H., Järvelin, A.I., Kammoun, M., Lee, J., Shuai, N., Garcia-Moreno, M., Andrejeva, A., et al. (2020). Global analysis of protein-RNA interactions in SARS-CoV-2 infected cells reveals key regulators of infection. bioRxiv. https://doi.org/10.1101/2020.11.25.398008.

Karam, B.S., Morris, R.S., Bramante, C.T., Puskarich, M., Zolfaghari, E.J., Lotfi-Emran, S., Ingraham, N.E., Charles, A., Odde, D.J., and Tignanelli, C.J. (2020). mTOR inhibition in COVID-19: A commentary and review of efficacy in RNA viruses. J. Med. Virol. *93*, 1843–1846. https://doi.org/10.1002/jmv.26728.

Kerns, J.A., Emerman, M., and Malik, H.S. (2008). Positive selection and increased antiviral activity associated with the PARP-containing isoform of human zinc-finger antiviral protein. PLoS Genet. *4*, e21.

Kerr, C.H., Skinnider, M.A., Andrews, D.D.T., Madero, A.M., Chan, Q.W.T., Stacey, R.G., Stoynov, N., Jan, E., and Foster, L.J. (2020). Dynamic rewiring of the human interactome by interferon signaling. Genome Biol. *21*, 140.

Kim, D., Lee, J.-Y., Yang, J.-S., Kim, J.W., Kim, V.N., and Chang, H. (2020a). The architecture of SARS-CoV-2 transcriptome. Cell *181*, 914–921.e10.

Kim, J.-M., Chung, Y.-S., Jo, H.J., Lee, N.-J., Kim, M.S., Woo, S.H., Park, S., Kim, J.W., Kim, H.M., and Han, M.-G. (2020b). Identification of coronavirus isolated from a patient in Korea with COVID-19. Osong Public Health Res. Perspect. *11*, 3–7.

Klann, K., Bojkova, D., Tascher, G., Ciesek, S., Münch, C., and Cinatl, J. (2020). Growth Factor Receptor Signaling Inhibition Prevents SARS-CoV-2 Replication. Mol. Cell *80*, 164–174. https://doi.org/10.1016/j.molcel.2020.08.006.

Lahr, R.M., Fonseca, B.D., Ciotti, G.E., Al-Ashtal, H.A., Jia, J.-J., Niklaus, M.R., Blagden, S.P., Alain, T., and Berman, A.J. (2017). La-related protein 1 (LARP1) binds the mRNA cap, blocking eIF4F assembly on TOP mRNAs. eLife *6*, e24146.

Lai, M.M.C., and Cavanagh, D. (1997). The molecular biology of coronaviruses. In Advances in Virus Research, K. Maramorosch, F.A. Murphy, and A.J. Shatkin, eds. (San Diego: Academic Press), pp. 1–100.

Lai, M.M., and Stohlman, S.A. (1981). Comparative analysis of RNA genomes of mouse hepatitis viruses. J. Virol. *38*, 661–670.

Lan, T.C.T., Allan, M.F., Malsick, L.E., Khandwala, S., Nyeo, S.S.Y., Bathe, M., Griffiths, A., and Rouskin, S. (2020). Structure of the full SARS-CoV-2 RNA genome in infected cells. bioRxiv. https://doi.org/10.1101/2020.06.29.178343.

Langmead, B., and Salzberg, S.L. (2012). Fast gapped-read alignment with Bowtie 2. Nat. Methods *9*, 357–359.

Lee, F.C.Y., and Ule, J. (2018). Advances in CLIP technologies for studies of protein-RNA interactions. Mol. Cell *69*, 354–369.

Lee, A.S., Kranzusch, P.J., Doudna, J.A., and Cate, J.H.D. (2016). eIF3d is an mRNA cap-binding protein that is required for specialized translation initiation. Nature *536*, 96–99.

Lee, K.-M., Chen, C.-J., and Shih, S.-R. (2017). Regulation mechanisms of viral IRES-driven translation. Trends Microbiol. *25*, 546–561.

Li, L., Zhao, H., Liu, P., Li, C., Quanquin, N., Ji, X., Sun, N., Du, P., Qin, C.-F., Lu, N., and Cheng, G. (2018). *PARP12* suppresses Zika virus infection through PARP-dependent degradation of NS1 and NS3 viral proteins. Sci. Signal. *11*, eaas9332.

Manokaran, G., Finol, E., Wang, C., Gunaratne, J., Bahl, J., Ong, E.Z., Tan, H.C., Sessions, O.M., Ward, A.M., Gubler, D.J., et al. (2015). Dengue subgenomic RNA binds TRIM25 to inhibit interferon expression for epidemiological fitness. Science *350*, 217–221.

Masutani, M., Sonenberg, N., Yokoyama, S., and Imataka, H. (2007). Reconstitution reveals the functional core of mammalian eIF3. EMBO J. *26*, 3373–3383.

McHugh, C.A., and Guttman, M. (2018). RAP-MS: a method to identify proteins that interact directly with a specific RNA molecule in cells. Methods Mol. Biol. *1649*, 473–488.

McHugh, C.A., Chen, C.-K., Chow, A., Surka, C.F., Tran, C., McDonel, P., Pandya-Jones, A., Blanco, M., Burghard, C., Moradian, A., et al. (2015). The Xist lncRNA interacts directly with SHARP to silence transcription through HDAC3. Nature *521*, 232–236.

Miknis, Z.J., Donaldson, E.F., Umland, T.C., Rimmer, R.A., Baric, R.S., and Schultz, L.W. (2009). Severe acute respiratory syndrome coronavirus nsp9 dimerization is essential for efficient viral growth. J. Virol. *83*, 3007–3018.

Mukherjee, J., Hermesh, O., Eliscovich, C., Nalpas, N., Franz-Wachtel, M., Maček, B., and Jansen, R.-P. (2019). β-Actin mRNA interactome mapping by proximity biotinylation. Proc. Natl. Acad. Sci. U S A *116*, 12863–12872.

Narayanan, K., Huang, C., Lokugamage, K., Kamitani, W., Ikegami, T., Tseng, C.-T.K., and Makino, S. (2008). Severe acute respiratory syndrome coronavirus nsp1 suppresses host gene expression, including that of type I interferon, in infected cells. J. Virol. *82*, 4471–4479.

Ooi, Y.S., Majzoub, K., Flynn, R.A., Mata, M.A., Diep, J., Li, J.K., van Buuren, N., Rumachik, N., Johnson, A.G., Puschnik, A.S., et al. (2019). An RNA-centric dissection of host complexes controlling flavivirus infection. Nat. Microbiol. *4*, 2369–2382.

Peiris, J.S.M., Lai, S.T., Poon, L.L.M., Guan, Y., Yam, L.Y.C., Lim, W., Nicholls, J., Yee, W.K.S., Yan, W.W., Cheung, M.T., et al.; SARS study group (2003). Coronavirus as a possible cause of severe acute respiratory syndrome. Lancet *361*, 1319–1325.

Perez-Riverol, Y., Csordas, A., Bai, J., Bernal-Llinares, M., Hewapathirana, S., Kundu, D.J., Inuganti, A., Griss, J., Mayer, G., Eisenacher, M., et al. (2019). The PRIDE database and related tools and resources in 2019: improving support for quantification data. Nucleic Acids Res. *47* (D1), D442–D450.

Perlman, S., and Netland, J. (2009). Coronaviruses post-SARS: update on replication and pathogenesis. Nat. Rev. Microbiol. *7*, 439–450.

Ramanathan, M., Porter, D.F., and Khavari, P.A. (2019). Methods to study RNA-protein interactions. Nat. Methods *16*, 225–234.

Riva, L., Yuan, S., Yin, X., Martin-Sancho, L., Matsunaga, N., Pache, L., Burgstaller-Muehlbacher, S., De Jesus, P.D., Teriete, P., Hull, M.V., et al. (2020). Discovery of SARS-CoV-2 antiviral drugs through large-scale compound repurposing. Nature *586*, 113–119.

Rogers, G.W., Jr., Richter, N.J., Lima, W.F., and Merrick, W.C. (2001). Modulation of the helicase activity of eIF4A by eIF4B, eIF4H, and eIF4F. J. Biol. Chem. *276*, 30914–30922.

Roth, A., and Diederichs, S. (2015). Molecular biology: Rap and chirp about X inactivation. Nature *521*, 170–171.

Sa Ribero, M., Jouvenet, N., Dreux, M., and Nisole, S. (2020). Interplay between SARS-CoV-2 and the type I interferon response. PLoS Pathog. *16*, e1008737.

Schmidt, N., Lareau, C.A., Keshishian, H., Ganskih, S., Schneider, C., Hennig, T., Melanson, R., Werner, S., Wei, Y., Zimmer, M., et al. (2021). The SARS-CoV-2 RNA-protein interactome in infected human cells. Nat. Microbiol. *6*, 339–353.

Shah, K., McCormack, C.E., and Bradbury, N.A. (2014). Do you know the sex of your cells? Am. J. Physiol. Cell Physiol. *306*, C3–C18.

Shaw, A.E., Hughes, J., Gu, Q., Behdenna, A., Singer, J.B., Dennis, T., Orton, R.J., Varela, M., Gifford, R.J., Wilson, S.J., and Palmarini, M. (2017). Fundamental properties of the mammalian innate immune system revealed by multispecies comparison of type I interferon responses. PLoS Biol. *15*, e2004086.

Shi, M., Wang, L., Fontana, P., Vora, S., Zhang, Y., Fu, T.-M., Lieberman, J., and Wu, H. (2020). SARS-CoV-2 Nsp1 suppresses host but not viral translation through a bipartite mechanism. bioRxiv. https://doi.org/10.1101/2020.09.18.302901.

Sims, A.C., Burkett, S.E., Yount, B., and Pickles, R.J. (2008). SARS-CoV replication and pathogenesis in an in vitro model of the human conducting airway epithelium. Virus Res. *133*, 33–44.

Snijder, E.J., Decroly, E., and Ziebuhr, J. (2016). The nonstructural proteins directing coronavirus RNA synthesis and processing. Adv. Virus Res. *96*, 59–126.

Sola, I., Almazán, F., Zúñiga, S., and Enjuanes, L. (2015). Continuous and discontinuous RNA synthesis in coronaviruses. Annu. Rev. Virol. *2*, 265–288.

St-Germain, J.R., Astori, A., and Samavarchi-Tehrani, P. (2020). A SARS-CoV-2 BioID-based virus-host membrane protein interactome and virus peptide compendium: new proteomics resources for COVID-19 research. bioRxiv. https://doi.org/10.1101/2020.08.28.269175.

Stark, C., Breitkreutz, B.-J., Reguly, T., Boucher, L., Breitkreutz, A., and Tyers, M. (2006). BioGRID: a general repository for interaction datasets. Nucleic Acids Res. *34*, D535–D539.

Sutton, G., Fry, E., Carter, L., Sainsbury, S., Walter, T., Nettleship, J., Berrow, N., Owens, R., Gilbert, R., Davidson, A., et al. (2004). The nsp9 replicase protein of SARS-coronavirus, structure and functional insights. Structure *12*, 341–353.

Suzuki, Y., Chin, W.-X., Han, Q., Ichiyama, K., Lee, C.H., Eyo, Z.W., Ebina, H., Takahashi, H., Takahashi, C., Tan, B.H., et al. (2016). Characterization of RyDEN (C19orf66) as an interferon-stimulated cellular inhibitor against dengue virus replication. PLoS Pathog. *12*, e1005357.

Takata, M.A., Gonçalves-Carneiro, D., Zang, T.M., Soll, S.J., York, A., Blanco-Melo, D., and Bieniasz, P.D. (2017). CG dinucleotide suppression enables antiviral defence targeting non-self RNA. Nature *550*, 124–127.

Tauber, D., Tauber, G., Khong, A., Van Treeck, B., Pelletier, J., and Parker, R. (2020). Modulation of RNA condensation by the DEAD-box protein eIF4A. Cell *180*, 411–426.e16.

Tcherkezian, J., Cargnello, M., Romeo, Y., Huttlin, E.L., Lavoie, G., Gygi, S.P., and Roux, P.P. (2014). Proteomic analysis of cap-dependent translation identifies LARP1 as a key regulator of 5'TOP mRNA translation. Genes Dev. *28*, 357–371.

Terrazzano, G., Rubino, V., Palatucci, A.T., Giovazzino, A., Carriero, F., and Ruggiero, G. (2020). An Open Question: Is It Rational to Inhibit the mTor-Dependent Pathway as COVID-19 Therapy? Front. Pharmacol. *11*, 856. https://doi.org/10.3389/fphar.2020.00856.

Thoms, M., Buschauer, R., Ameismeier, M., Koepke, L., Denk, T., Hirschenberger, M., Kratzat, H., Hayn, M., Mackens-Kiani, T., Cheng, J., et al. (2020). Structural basis for translational shutdown and immune evasion by the Nsp1 protein of SARS-CoV-2. Science *369*, 1249–1255.

Tidu, A., Janvier, A., Schaeffer, L., Sosnowski, P., Kuhn, L., Hammann, P., Westhof, E., Eriani, G., and Martin, F. (2020). The viral protein NSP1 acts as a ribosome gatekeeper for shutting down host translation and fostering SARS-CoV-2 translation. RNA *27*, 253–264.

Ule, J., Hwang, H.-W., and Darnell, R.B. (2018). The future of cross-linking and immunoprecipitation (CLIP). Cold Spring Harb. Perspect. Biol. *10*, a032243.

UniProt Consortium (2019). UniProt: a worldwide hub of protein knowledge. Nucleic Acids Res. *47* (D1), D506–D515.

Van Nostrand, E.L., Freese, P., Pratt, G.A., Wang, X., Wei, X., Xiao, R., Blue, S.M., Chen, J.-Y., Cody, N.A.L., Dominguez, D., et al. (2020). A large-scale binding and functional map of human RNA-binding proteins. Nature *583*, 711–719.

Vijgen, L., Keyaerts, E., Moës, E., Thoelen, I., Wollants, E., Lemey, P., Vandamme, A.-M., and Van Ranst, M. (2005). Complete genomic sequence of human coronavirus OC43: molecular clock analysis suggests a relatively recent zoonotic coronavirus transmission event. J. Virol. *79*, 1595–1604.

Wang, X., Xuan, Y., Han, Y., Ding, X., Ye, K., Yang, F., Gao, P., Goff, S.P., and Gao, G. (2019). Regulation of HIV-1 Gag-Pol expression by shiftless, an inhibitor of programmed-1 ribosomal frameshifting. Cell *176*, 625–635.e14.

Wei, J., Alfajaro, M.M., DeWeirdt, P.C., Hanna, R.E., Lu-Culligan, W.J., Cai, W.L., Strine, M.S., Zhang, S.-M., Graziano, V.R., Schmitz, C.O., et al. (2021). Genome-wide CRISPR screens reveal host factors critical for SARS-CoV-2 infection. Cell *184*, 76–91.e13.

Welsby, I., Hutin, D., Gueydan, C., Kruys, V., Rongvaux, A., and Leo, O. (2014). PARP12, an interferon-stimulated gene involved in the control of protein translation and inflammation. J. Biol. Chem. *289*, 26642–26657.

Woo, P.C.Y., Lau, S.K.P., Lam, C.S.F., Lau, C.C.Y., Tsang, A.K.L., Lau, J.H.N., Bai, R., Teng, J.L.L., Tsang, C.C.C., Wang, M., et al. (2012). Discovery of seven novel Mammalian and avian coronaviruses in the genus deltacoronavirus supports bat coronaviruses as the gene source of alphacoronavirus and betacoronavirus and avian coronaviruses as the gene source of gammacoronavirus and deltacoronavirus. J. Virol. *86*, 3995–4008.

Zheng, X., Wang, X., Tu, F., Wang, Q., Fan, Z., and Gao, G. (2017). TRIM25 is required for the antiviral activity of zinc finger antiviral protein. J. Virol. *91*, e00088-17.

Zhou, P., Yang, X.-L., Wang, X.-G., Hu, B., Zhang, L., Zhang, W., Si, H.-R., Zhu, Y., Li, B., Huang, C.-L., et al. (2020). A pneumonia outbreak associated with a new coronavirus of probable bat origin. Nature *579*, 270–273.

Zhu, Y., Chen, G., Lv, F., Wang, X., Ji, X., Xu, Y., Sun, J., Wu, L., Zheng, Y.-T., and Gao, G. (2011). Zinc-finger antiviral protein inhibits HIV-1 infection by selectively targeting multiply spliced viral mRNAs for degradation. Proc. Natl. Acad. Sci. U S A *108*, 15834–15839.

Zhu, Y., Wang, X., Goff, S.P., and Gao, G. (2012). Translational repression precedes and is required for ZAP-mediated mRNA decay. EMBO J. *31*, 4236–4246.

STAR★METHODS

KEY RESOURCES TABLE

REAGENT or RESOURCE	SOURCE	IDENTIFIER
Antibodies		
Anti-SARS Coronavirus Nucleocapsid antibody	Invitrogen	Cat# PA1-41098; RRID: AB_1087200
Anti-RPS7 antibody	Abcam	Cat#ab57637; RRID: AB_945322
Anti-Coronavirus antibody, OC-43 strain, clone 541-8	Merck	Cat#MAB9012; RRID: AB_95424
Anti-GAPDH antibody (6C5)	Abcam	Cat#ab8245; RRID: AB_2107448
Anti-LARP1 antibody	Bethyl	Cat# A302-087A; RRID: AB_1604274
Anti-ZC3HAV1(ZAP) antibody	Invitrogen	Cat# PA5-31650; RRID: AB_2549123
Anti-C19orf66 (SHFL) antibody	Abcam	Cat# ab122765; RRID: AB_11129894
Anti-GFP antibody	Abcam	Cat# ab290; RRID: AB_303395
Anti-FLAG antibody	Sigma-Aldrich	Cat# F3165; RRID: AB_259529
Bacterial and virus strains		
SARS-CoV-2	National Culture Collection for Pathogens, Korea National Institute of Health, Korea	NCCP 43326
HCoV-OC-43	Korea Bank for Pathogenic Viruses	KBPV-VR-8
Chemicals, peptides, and recombinant proteins		
Antibiotic-Antimycotic	GIBCO	Cat#15240-062
TRIzol	Invitrogen	Cat#15596-018
TRIzol LS	Invitrogen	Cat#10296-028
DMEM, High glucose	Welgene	Cat#LM001-05
RPMI 1640, HEPES	Welgene	Cat#LM011-03
FBS	GIBCO	Cat#10082147
TURBO DNase I	Invitrogen	Cat#AM2239
QiAquick PCR purification kit	QIAGEN	Cat#28106
RNase-Free DNase Set	QIAGEN	Cat#79254
RNeasy Mini Kit	QIAGEN	Cat#74106
RevertAid Reverse Transcriptase	Thermo Scientific	Cat#EP0442
MEGAscript T7 Transcription Kit	Invitrogen	Cat#AMB13345
AMPure XP	Beckman	Cat#A63881
RNAClean XP	Beckman	Cat#A63987
SUPERase●In RNase Inhibitor	Invitrogen	Cat#AM2696
Streptavidin magnetic beads	New England Biolabs	Cat#S1420S
Proteinase K	Roche	Cat#03 115 879 001
Lithium chloride 8 M solution	Sigma	Cat#L7026
Lithium dodecyle sulfate	Sigma	Cat#L9781
Urea	Sigma	Cat#U6504
Poly(ethylene glycol)	Sigma	Cat#P3015
Iodoacetamide	Sigma	Cat#I1149
Sodium hydroxide solution	Sigma	Cat#72068
Ammonium bicarbonate	Sigma	Cat#09830
DTT	Thermo Scientific	Cat#R0861
Acetic acid (glacial) 100%	Merck	Cat#100063
Tris-Cl pH 7.0	Invitrogen	Cat#AM9851
Tris-Cl pH 8.0	Invitrogen	Cat#AM9856

(*Continued on next page*)

Continued

REAGENT or RESOURCE	SOURCE	IDENTIFIER
EDTA (0.5 M), pH 8.0, RNase-free	Invitrogen	Cat#AM9261
GlycoBlue	Invitrogen	Cat#AM9516
PowerSYBR Green PCR Master Mix	Applied Biosystems	Cat#AB4367659
KAPA HiFi Hot Start ReadyMix PCR kit	Roche	Cat#KK2602
DEPC-treated Water	Invitrogen	Cat#4387937
Pierce Trypsin Protease, MS Grade	Thermo Scientific	Cat#90058
Benzonase® Nuclease	Millipore	Cat#E1014
Direct-zol RNA Miniprep	Zymo Research	Cat#R2051
HiPPR Detergent Removal Spin Columns, 0.1 mL	Thermo Scientific	Cat#88305
HyperSep C18 Cartridges	Thermo Scientific	Cat#60108
Novex WedgeWell 10 to 20%, Tris-Glycine, 1.0 mm, Mini Protein Gel, 15-well	Invitrogen	Cat#XP10205BOX
PageRuler Plus Prestained Protein Ladder	Thermo Scientific	Cat#26619
Lipofectamine RNAiMAX Transfection Reagent	Invitrogen	Cat#13778150
Fugene HD Transfection agent	Promega	Cat#E2312
DMSO	Sigma	Cat#D2650
Rapamycin	AG Scientific	Cat#R-1018
Critical commercial assays		
EzWay Protein-Silver Staining Kit	KOMA Biotech	Cat#K14040D
CellTiter 96® Non-Radioactive Cell Proliferation Assay (MTT)	Promega	G4000
Deposited data		
Raw and analyzed data	This manuscript	PRIDE: PXD024808
SARS-CoV-2 transcriptome data	Blanco-Melo et al., 2020	GEO: GSE147507
Protein-protein interaction data	Stark et al., 2006	Release 3.5.187
Subcellular localization data	Go et al., 2019	Human cell map database v1
Pfam database	El-Gebali et al., 2019	Version 33.1
Original images and supplemtal tables	This manuscript	Mendeley Data: https://dx.doi.org/10.17632/7fgg5452pr.1
Experimental models: Cell lines		
Vero	ATCC	CCL-81; RRID:CVCL_0059
HCT-8	KCLB	10244; RRID:CVCL_2478
Calu-3	KCLB	30055; RRID:CVCL_0609
Lenti-X 293T Cell Line	Takara Bio	632180
Oligonucleotides		
Pooled oligo for probe generation	Custom Array	See Table S1 Custom Array
PCR primers	BIONICS	See Table S1 PCR primer
SMARTpool siRNA	Horizon Discovery	See Table S1 siRNA
Recombinant DNA		
pCK-FLAG-AcGFP	This manuscript	N/A
pCI4-FLAG-SFHL	This manuscript	N/A
pCI4-FLAG-LARP1	This manuscript	N/A
p3XFLAG-CMV14 ZAPS	This manuscript (Gift from Dr. Kwangseog Ahn)	N/A
p3XFLAG-CMV14 ZAPL	This manuscript (Gift from Dr. Kwangseog Ahn)	N/A

(*Continued on next page*)

Continued

REAGENT or RESOURCE	SOURCE	IDENTIFIER
Software and algorithms		
MaxQuant	https://www.maxquant.org/	version 1.6.15.0
Bowtie2	http://bowtie-bio.sourceforge.net/bowtie2/index.shtml	version 2.3.5
R	https://www.r-project.org/	version 3.6.1
The tidyverse R package	https://www.tidyverse.org/	version 1.3.0
The topGO R package	Alexa et al., 2006	version 2.36.0
The ggrepel R package	https://cran.r-project.org/web/packages/ggrepel/	version 0.8.2
The UpSetR R package	https://cran.r-project.org/web/packages/UpSetR/	version 1.4.0

RESOURCE AVAILABILITY

Lead contact

Further information and requests for resources and reagents should be directed to and will be fulfilled by the lead contact, V. Narry Kim (narrykim@snu.ac.kr)

Material availability

All reagents generated in this study are available from the lead contact upon request.

Data and code availability

The proteomics data have been deposited to the ProteomeXchange Consortium via the PRIDE (Perez-Riverol et al., 2019) partner repository with the dataset identifier PXD024808.

EXPERIMENTAL MODEL AND SUBJECT DETAILS

Cell lines

All 4 cell lines used in this study (HCT-8, male; Lenti-X 293T, female; Calu-3, male; Vero) (Shah et al., 2014) were maintained in culture media supplemented with 10% FBS and 1 × Antibiotic-Aintimycotic solution (GIBCO) and routinely cultured at 37°C with 5% CO_2. FBS were thawed in a 37°C water bath and were not heat-inactivated. RPMI 1640 with HEPES (Welgene, LM011-03) were used when culturing HCT-8 while DMEM with high glucose (Welgene, LM001-05) were used for Vero, Calu-3, and Lenti-X 293T cells. During virus infection for both SARS-CoV-2 and HCoV-OC43, the serum concentration was reduced to final 2%. During the infection of HCoV-OC43, the temperature for HCT-8 was lowered to 35°C. PCR test results for mycoplasma contamination were negative for all 4 cell lines (Test order through Bionics, Korea). Cell line authentication for Lenti-X 293T by short tandem repeat (STR) analysis reported 100% match to 293T (CRL-3216), according to the service requested through ATCC (ATCC sales order: SO0054768). 3 other purchased cell lines were morphologically evaluated for their cell identity without STR tests.

Human samples

RNA sequencing data from human patients were downloaded from publicly available database from the published work (Blanco-Melo et al., 2020). No samples from human subjects were used in this study.

Animal models

No animal experiments were performed in this study.

METHOD DETAILS

Preparation of antisense oligonucleotide templates

By scanning the genomic RNAs of SARS-CoV-2 (NCBI RefSeq accession NC_045512.2) and HCoV-OC43 (GenBank accession AY391777.1) from head to tail, partially overlapping 90 nt tiles were enumerated. These tiles were designed to have 30 nt spacing, so adjacent tiles share a subsequence of 60 nt. To avoid ambiguous targeting, tiles were aligned to the human transcriptome (version of Oct 14, 2019) using bowtie 2 (Langmead and Salzberg, 2012) and multi-mapped sequences were discarded. To prepare biotinylated antisense oligonucleotides (ASOs) in bulk, the sequence elements for *in vitro* transcription (IVT), reverse transcription (RT) and PCR were added to the 90 nt tiles. The T7 promoter (5′-TAA TAC GAC TCA CTA TAG GG-3′) and a pad for RT priming

(5′-TGG AAT TCT CGG GTG CCA AGG-3′) were added to the head and tail of each tile, respectively. We grouped ASOs into two sets for each viral genome: "Probe I" targets the unique region of genomic RNA ([265:21553] of NC_045512.2; [:21506] of AY391777.1) and "Probe II" aims at both genomic and subgenomic RNAs ([21562:] of NC_045512.2; [21506:] of AY391777.1). The templates of four ASO groups have distinct PCR primer binding sites on both ends. Accordingly, each ASO set can be selectively amplified from a single mixture. The final ASO templates (167 nt) were prepared via the oligo pool synthesis service of Genscript and stored at −80°C. The ASO templates used in this study are listed in Table S1.

Mass production of biotin-labeled ASO

ASO templates were amplified using KAPA HiFi HotStart ReadyMix (Roche) and PCR primers for an ASO pool. PCR products were purified by QIAquick PCR purification kit (QIAGEN). RNA intermediates were then transcribed using MEGAscript T7 transcription kit (Invitrogen), and DNA templates were degraded by TURBO DNase (Invitrogen). To clean up enzymes and other reagents, 1.8X reaction volume of AMPure XP (Beckman) was applied and polyethylene glycol was added to be final 20%. The size selection was carried out according to the manufacturer's protocol. Biotinylated ASOs were synthesized by RevertAid Reverse Transcriptase (Thermo Scientific) and 5′ biotin-TEG primer. RNA intermediates were hydrolyzed at 0.1 M NaOH and neutralized with acetic acid. Finally, ASO purification was performed in the same manner as IVT RNA selection. The primer sequences used for PCR and reverse transcription are listed in Table S1.

Compilation of proteome databases

The Uniprot reference proteome sets for human (UP000005640, canonical, SwissProt) and African green monkey (Chlorocebus sabaeus; UP000029965, canonical, SwissProt and TrEMBL) were used to identify host proteins in each mass spectrometry experiment (version 03/21/2020) (UniProt Consortium, 2019). The reference proteome set for the Severe acute respiratory syndrome coronavirus 2 (SARS-CoV-2) was manually curated largely based on the NCBI Reference Sequence (NC_045512.2) and related literature of other accessory proteins (e.g., ORF3b, ORF9b and ORF9c). The reference proteome set for the Human coronavirus OC43 (HCoV-OC43) was compiled based on the Uniprot Swiss-Prot proteins for HCoV-OC43 (taxonomy:31631) except for HCoV-OC43 Protein I which was separated into Protein Ia and Protein Ib (or N2) (Vijgen et al., 2005).

Cell culture, transfection and virus infection

Virus experiments were carried out in accordance with the biosafety guideline by the Korea Centers for Disease Control & Prevention (KCDC). The Institutional Biosafety Committee of Seoul National University (SNUIBC) approved the protocols used in this study, including SNUIBC-R200331-1-1 for BL2 experiments and SNUIBC-200508-1 for BL3 experiments. Vero and HCT-8 cells were maintained in DMEM (Welgene) and RPMI 1640 (Welgene) respectively, both with 1 × Antibiotic-Antimycotic (GIBCO) and 10% FBS (GIBCO) and cultured in CO_2 incubator with 5% CO_2 at 37 C. For SARS-CoV-2 infection, 7×10^6 Vero cells were plated in T-175 flasks 24 hours before infection. Cells were washed with serum-free media and incubated with 5 mL virus-diluted media for 30 minutes at 0.1 MOI, as determined by plaque assay. After infection, virus containing media was replaced with reduced-serum media (2% FBS) and cultured until the harvest. For HCoV-OC43 infection, a similar protocol was used except for incubation temperature lowered to 33 C. For siRNA transfection, 3.5×10^5 Calu-3 cells, maintained in DMEM with 1X Antibiotic-Antimycotic and 10% FBS in CO_2 incubator with 5% CO_2 at 37 C, were plated in 12 well plate and final 50 nM siRNAs were reverse-transfected using Lipofectamine RNAiMAX (Invitrogen) and ON-TARGETplus SMARTpool siRNAs (Horizon Discovery). Cell viability after siRNA knockdown was measured by splitting $1/100^{th}$ of cells from uninfected cells, 48 hours after transfection into 96 well plates in triplicates and cell number was measured by MTT assay (Promega) at 4 hours after addition of tetrazolium dye.

For overexpression experiments, CDS sequences were PCR amplified from Calu-3 cDNA and cloned into pCI4-FLAG vector for SHFL, and LARP1. Plasmids for two isoforms of ZC3HAV1 (p3XFLAG-CMV14 ZC3HAV1-S or ZC3HAV1-L) were kindly provided by Gwangseog Ahn's lab at SNU. 2×10^5 293T cells were plated in 24 well plate 18 hours before transfection and 1 ug plasmid DNA was mixed with 3 uL of FuGENE HD (Promega). After 24 hours for protein expression, cells were infected with SARS-CoV-2 at 0.5 MOI.

RNA purification and RT-qPCR

For total RNA purification from virus-infected cells, 1 mL TRIzol LS (Invitorgen) were added to media-removed cell monolayers per single well of 12 well plates followed by on-column DNA digestion and purification (Zymo Research). For RNA purification from RNP capture sample, bead-captured RNAs were digested with 100 ng Proteinase K (PCR grade, Roche) and incubated at 37°C for 1 hour, followed by RNA isolation by TRIzol LS with GlycoBlue (Invitrogen). 1∼5 μg RNA were reverse-transcribed using RevertAid transcriptase (Thermo Scientific) and random hexamer. qPCR was performed with primer pairs listed in Table S1 and PowerSYBR Green (Applied Biosystems) and analyzed with QuantStudio 5 (Thermo Scientific).

Modified RNA antisense purification coupled with mass spectrometry (RAP-MS)

Virus infected cells were detached from culture vessels by trypsin and cell pellets were resuspended with ice-cold PBS in order to avoid RNA degradation during UV cross-linking on plastic culture vessels. We found RNA degradation is exacerbated when flat adhesion cells were irradiated directly on the cultured dish. 12 mL cell suspensions were dispersed in 150 mm dishes to irradiate 254 nm

UV for 2.5 J/cm^2 using BIO-LINK BLX-254 for SARS-CoV-2 or 0.8 J/cm^2 using Spectrolinker XL-1500 for HCoV-OC43. UV-cross-linked cells were pelleted by centrifugation and resuspended in TURBO DNase solution (150 Units per flask) and incubated at 37°C for 30 minutes. DNA digested cells were supplemented with equal volume of pre-heated 2X lysis buffer (40 mM Tris-Cl at pH 7.5, 1 M LiCl, 1% LDS, 2 mM EDTA, 10 mM DTT and 8 M urea) and denatured by incubating at 68°C for 30 minutes. Per replicate, cell lysate from 1 flask (T-175) were mixed with 20 μg biotin probe pools (Probe I or Probe II) and hybridized by incubating at 68°C for 30 minutes in final 1 mL volume. Biotin-labeled RNP lysates were supplemented with streptavidin beads (1 mL per replicate, New England Biolabs) and captured by rotating at room temperature overnight. Probe-enriched RNP beads were washed with 1X lysis buffer twice and transferred to fresh tubes, followed by final wash with detergent-free wash buffer (20 mM Tris-Cl at pH 7.5, 0.5 M LiCl, 1 mM EDTA). 1/10th of beads were set aside for assessment of RNA contents by RT-qPCR and another 1/10th of beads were used for silver staining (KOMA biotech). The remaining 8/10th of beads were digested with 100 units of Benzonase nuclease (Millipore) at 37°C for 1 hour. For on-bead peptide digestion, nuclease treated beads were suspended to final 8 M urea and reduced with 10 mM dithiothreitol (DTT), alkylated with 40 mM iodoacetamide (IAA) for 1 hour each at 37°C, and diluted with 50 mM ammonium bicarbonate (ABC) to final 1 M urea. These bead suspensions were supplemented with 300 ng Trypsin (Thermo Scientific, MS grade) and 1 mM $CaCl_2$ and digested overnight at 37°C. Peptide solutions were separated from magnetic beads and further processed with HiPPR detergent removal spin columns (Thermo Scientific) and desalted by reverse phase C18 ziptip (Millipore). After the clean up and dry down, the samples were reconstituted with 20 μL of 25 mM ammonium bicarbonate buffer for LC-MS/MS analysis.

LC-MS/MS analysis

LC-MS/MS analysis was carried out using Orbitrap Fusion Lumos Tribrid MS (Thermo Fisher Scientific) coupled with nanoAcquity UPLC system (Waters). Both analytical capillary columns (100 cm x 75 μm i.d.) and the trap columns (3 cm x 150 μm i.d) were packed in-house with 3 μm Jupiter C18 particles (Phenomenex, Torrance). The long analytical column was placed in a column heater (Analytical Sales and Services) regulated to a temperature of 45°C. The LC flow rate was 300 nL/min and the 100-min linear gradient ranged from 95% solvent A (H_2O with 0.1% formic acid (Merck)) to 40% solvent B (100% acetonitrile with 0.1% formic acid). Precursor ions were acquired at 120 K resolving power at m/z 200 and the isolation of precursor for MS/MS analysis was performed with a 1.4 Th. Higher-energy collisional dissociation (HCD) with 30% collision energy was used for sequencing with a target value of 1E5 ions determined by automatic gain control. Resolving power for acquired MS2 spectra was set to 30 K at m/z 200 with 120 ms maximum injection time. The mass spectrometry proteomics data have been deposited to the ProteomeXchange Consortium via the PRIDE (Perez-Riverol et al., 2019) partner repository with the dataset identifier PXD024808.

Mass spectrometric raw data files were processed for Label-Free Quantification with MaxQuant (version 1.6.15.0) (Cox and Mann, 2008) using the built-in Andromeda search engine (Cox et al., 2011) at default settings with a few exceptions. Briefly, for peptide-spectrum match (PSM) search, cysteine carbamidomethylation was set as fixed modifications, and methionine oxidation and N-terminal acetylation were set as variable modifications. Tolerance for the first and main PSM search were 20 and 4.5 ppm, respectively. Peptides from common contaminant proteins were identified by utilizing the contaminant database provided by MaxQuant. FDR threshold of 1% was used for both the peptide and protein level. The match-between-runs option was enabled with default parameters in the identification step. Finally, LFQ was performed for those with a minimum ratio count of 1.

QUANTIFICATION AND STATISTICAL ANALYSIS

Statistical analysis for RNP capture experiment

To identify host and viral proteins that interact with the particular RNA species of interest (e.g., sgRNA or gRNA), we utilized the results from the "bead only" and "probe only" samples as technical backgrounds. Specifically, the "bead only" (or no-probe) experiment in infected cells was used to account for non-specific interactors and biotin-containing carboxylases (e.g., PCCA, ACACA, and ACACB) and determine the set of host and viral proteins that in a broad sense bind to the RNA, which we call Probe I/II "binding" proteins. The probe experiment in uninfected cells (i.e., "probe only") was then used as the technical background against target RNA-independent interactors and determine the set of host proteins that are enriched for the target RNA, which we call Probe I/II "enriched" proteins.

To accomplish this, we considered the protein spectra count data as a multinomial distribution and applied a statistical test for spectra count enrichment. This is analogous to modeling a bag of skittles and statistically identifying whether you received statistically more "green" skittles than random. In this study, the control samples were used to estimate the parameters of the multinomial distribution of the null hypothesis. In turn, this is normalizing the spectra count data by the total counts, and the basis for this is our multinomial modeling of the data generative process.

Specifically, let N_p be the number of identified spectra counts for protein group p from the case experiment (e.g., Probe I experiment in infected cells), and M_p be the respective count number from the control experiment (e.g., no-probe experiment in infected cells). For each protein i with $N_i \geq 1$, the statistical significance of enrichment is:

$$P(X \geq N_i) = \sum_{k=N_i}^{N} B(k; N, \theta_i)$$

$$\theta_i = \frac{M_i + 1}{\sum_i (M_i + 1)}$$

where $N = \sum N_i$ is the total spectra count, θ_i is the background probability, and $B(k\ ;\ n,\ p)$ is the binomial distribution of k successes in n trails with success probability p. Finally, the Benjamini-Hochberg method was used to adjust the p values and control the false discovery rate.

Gene Ontology (GO) enrichment analysis

We conducted enrichment analyses of Gene Ontology (GO) terms (Gene Ontology Consortium, 2001) by means of summarizing the function of tens of host proteins identified in the RNP capture experiment. In general, Fisher's exact test is used to estimate the statistical significance of the association (i.e., contingency) between a particular GO term and the gene set of interest. To improve the explanatory power of this analysis, we used the weight01 algorithm (Alexa et al., 2006) from the topGO R package which accounts for the GO graph structure and reduces local dependencies between GO terms. Detailed information of the Gene Ontology was from the GO.db R package (version 3.8.2), and GO gene annotations were from the org.Hs.eg.db R package (version 3.8.2).

Protein-protein interaction network analysis

We integrated protein-protein interaction data from the BioGRID database (Release 3.5.187) (Stark et al., 2006) and retrieved other proteins that do not necessarily bind to the SARS-CoV-2 RNA but form either transient or stable physical interactions with the host proteins identified from the RNP capture experiments. In detail, we considered only human protein-protein interactions that were (1) found from at least two different types of experiments and (2) reported by at least three publication records which resulted in a total of 65,625 interactions covering 12,143 human proteins. Physical interactions between SARS-CoV-2 proteins and human proteins were by affinity capture and mass spectrometry in SARS-CoV-2 protein expressing cells (Gordon et al., 2020). The network R package and the ggnet2 function of the GGally R package was used for graph visualization.

Protein domain enrichment analysis

Pfam database (version 33.1) (El-Gebali et al., 2019) was used for protein domain enrichment analysis. Taxon 9606 (human) and Taxon 60711 (green monkey) protein domain annotations were used to analyze RNP capture results of HCoV-OC43 and SARS-CoV-2, respectively. One-sided Fisher's exact test was applied to estimate the statistical enrichment of a particular protein domain for the specific gene set (e.g., SARS-CoV-2 Probe I binding proteins). We utilized the set of all proteins identified in the RNP capture experiments and all protein domains annotated to those proteins as the statistical background of the enrichment analysis.

Subcellular localization analysis

To investigate the subcellular localizations of the SARS-CoV-2 interactome, we leveraged the protein subcellular localization information from the Human cell map database v1 (Go et al., 2019). Information from the SAFE algorithm was used primarily but then supplemented by information from the NMF algorithm in case of "no prediction" or "-" localizations. Localization terms of the NMF algorithm were matched to terms of the SAFE algorithm in general, but few were mapped to the higher term of the SAFE algorithm. For example, the "cell junction" term of the NMF algorithm was merged to the "cell junction, plasma membrane" term of the SAFE algorithm.